

RESEARCH ARTICLE

A Nitric Oxide Regulated Small RNA Controls Expression of Genes Involved in Redox Homeostasis in *Bacillus subtilis*

Sylvain Durand¹, Frédérique Braun^{1‡}, Efthimia Lioliou^{2‡}, Cédric Romilly², Anne-Catherine Helfer², Laurianne Kuhn³, Noé Quittot⁴, Pierre Nicolas⁴, Pascale Romby^{2*}, Ciarán Condon^{1*}

1 CNRS FRE 3630 (affiliated with Univ. Paris Diderot, Sorbonne Paris Cité), Institut de Biologie Physico-Chimique, Paris, France, **2** Architecture et Réactivité de l'ARN, Université de Strasbourg, CNRS, IBMC, Strasbourg, France, **3** Plateforme Protéomique Esplanade, IBMC, Strasbourg, France, **4** Mathématique Informatique et Génome, INRA UR1077, Jouy en Josas, France

‡ These authors contributed equally to this work.

* condon@ibpc.fr (CC); p.romby@ibmc-cnrs.unistra.fr (PR)



 OPEN ACCESS

Citation: Durand S, Braun F, Lioliou E, Romilly C, Helfer AC, Kuhn L, et al. (2015) A Nitric Oxide Regulated Small RNA Controls Expression of Genes Involved in Redox Homeostasis in *Bacillus subtilis*. PLoS Genet 11(2): e1004957. doi:10.1371/journal.pgen.1004957

Editor: Danielle A. Garsin, The University of Texas Health Science Center at Houston, UNITED STATES

Received: October 21, 2014

Accepted: December 15, 2014

Published: February 2, 2015

Copyright: © 2015 Durand et al. This is an open access article distributed under the terms of the [Creative Commons Attribution License](https://creativecommons.org/licenses/by/4.0/), which permits unrestricted use, distribution, and reproduction in any medium, provided the original author and source are credited.

Data Availability Statement: All relevant data are within the paper and its Supporting Information files.

Funding: This work was supported by funds from the Centre National de la Recherche Scientifique to CNRS FRE3630 (CC) and CNRS UPR9002 (PR); web-site: <http://www.cnrs.fr>, Université Paris VII-Denis Diderot to FRE3630 (CC); web site: <http://www.univ-paris-diderot.fr> and the Agence Nationale de la Recherche ANR-12-BSV6-0007 asSUPYCO (CC); ANR-11-LABX-0011-01 DYNAMO (CC); ANR-10-LABX-0036_NETRINA (PR); web site: <http://www.agence-nationale-recherche.fr>. CR was supported by

Abstract

RsaE is the only known *trans*-acting small regulatory RNA (sRNA) besides the ubiquitous 6S RNA that is conserved between the human pathogen *Staphylococcus aureus* and the soil-dwelling Firmicute *Bacillus subtilis*. Although a number of RsaE targets are known in *S. aureus*, neither the environmental signals that lead to its expression nor its physiological role are known. Here we show that expression of the *B. subtilis* homolog of RsaE is regulated by the presence of nitric oxide (NO) in the cellular milieu. Control of expression by NO is dependent on the ResDE two-component system in *B. subtilis* and we determined that the same is true in *S. aureus*. Transcriptome and proteome analyses revealed that many genes with functions related to oxidative stress and oxidation-reduction reactions were up-regulated in a *B. subtilis* strain lacking this sRNA. We have thus renamed it RoxS. The prediction of RoxS-dependent mRNA targets also suggested a significant enrichment for mRNAs related to respiration and electron transfer. Among the potential direct mRNA targets, we have validated the *ppnKB* mRNA, encoding an NAD⁺/NADH kinase, both *in vivo* and *in vitro*. RoxS controls both translation initiation and the stability of this transcript, in the latter case *via* two independent pathways implicating RNase Y and RNase III. Furthermore, RNase Y intervenes at an additional level by processing the 5' end of the RoxS sRNA removing about 20 nucleotides. Processing of RoxS allows it to interact more efficiently with a second target, the *sucCD* mRNA, encoding succinyl-CoA synthase, thus expanding the repertoire of targets recognized by this sRNA.

the Fondation de la Recherche Médicale; web site: <http://www.frm.org/>. The funders had no role in study design, data collection and analysis, decision to publish, or preparation of the manuscript.

Competing Interests: The authors have declared that no competing interests exist.

Author Summary

Bacteria have evolved various strategies to continually monitor the redox state of the internal and external environments to prevent cell damage and/or to protect them from host defense mechanisms. These signals modify the expression of genes, allowing bacteria to adapt to altered redox environments and to maintain homeostasis. Studies in *Enterobacteriaceae* have shown that sRNAs play central roles in adaptation to oxidative stress. We show here that the conserved sRNA, RoxS is induced by the presence of nitric oxide (NO) in the medium, through the ResDE and SrrAB two-component systems of *Bacillus subtilis* and *Staphylococcus aureus*, respectively. *B. subtilis* RoxS regulates functions related to oxidation-reduction reactions and acts as an antisense RNA to control translation initiation and the degradation of *ppnKB* mRNA, encoding an NAD⁺/NADH kinase. Interestingly, RNase Y processes the 5' end of the RoxS sRNA leading to a truncated sRNA that in turn interacts more efficiently with a second target, the *sucCD* mRNA, encoding succinyl-CoA synthase. Taken together this work shows that RoxS is part of a complex regulatory network that allows the cell to sense and respond to redox perturbations, and revealed a novel process that allows an expansion of the repertoire of sRNA targets.

Introduction

Small regulatory RNAs (sRNA) have been shown to play key roles in the regulation of a wide variety of cellular processes in bacteria, including stress responses, environmental signaling and virulence [1,2]. They generally regulate at the post-transcriptional level by altering mRNA translation or stability. Most sRNAs identified to date base pair with the 5' untranslated region (5'-UTR) and alter ribosome binding to the mRNA. Changes in translation rates often have indirect consequences for mRNA stability as ribosomes can shield mRNA from attack by ribonucleases. A number of sRNAs have also been shown to directly affect mRNA stability without altering translation initiation rates through interactions with the 5'-UTR, the 3'-UTR or the coding sequence [3,4,5,6].

Although bacterial sRNAs have been studied most extensively in *Escherichia coli* and closely related organisms, the link to virulence has led to the identification and characterization of sRNAs in a wide range of both Gram-negative and Gram-positive bacterial pathogens. The Gram-positive model organism *Bacillus subtilis* trails conspicuously behind in these efforts, where only two *trans*-acting sRNAs, SR1 and FsrA, have been studied in detail [7–11]. The RNA chaperone Hfq has been shown to play a key role in sRNA association with its mRNA target in Proteobacteria. However, its role in Firmicutes seems to be less evident [7,8,12–14], suggesting that alternative RNA chaperones remain to be discovered in these organisms. Furthermore, there are important differences in the mRNA degradation machineries and pathways of these two bacterial clades, most notably the widespread occurrence of a 5'-3' exoribonuclease activity provided by RNase J in the Firmicutes and the ability of stalled ribosomes to protect long stretches of downstream mRNA from ribonucleolytic attack [15,16]. The RNases involved in the regulation of mRNA stability by sRNAs in the Firmicutes have not been identified in many cases.

RsaE was first discovered in *Staphylococcus aureus* as a member of a family of sRNAs that contain multiple C-rich regions (CRR) that can potentially pair with the G-rich Shine Dalgarno (SD) sequences of ribosome binding sites to inhibit translation [17]. RsaE shows some strain-dependence in its expression patterns [17,18], but in all tested clinical isolates expression of RsaE was maximal during mid-exponential growth and declined in late-exponential/pre-stationary

phase [19]. Expression of RsaE in *S. aureus* strain RN6390 was activated by the *agr* quorum sensing system that plays a key role in *S. aureus* virulence [17] and was further shown to be induced by both oxidative stress and high salt conditions [17,18]. Transcriptome and proteome analysis of RsaE deletion strains or overexpressing strains pointed to a role for *S. aureus* RsaE in governing the expression of genes involved in central metabolism, notably folate metabolism and the TCA cycle [17,18].

RsaE is highly conserved between *Bacillus* and *Staphylococcus* species at both the primary sequence and predicted secondary structure level [17] (Fig. 1A). The two best-studied representatives of these groups, *B. subtilis* and *S. aureus*, occupy very different ecological niches, the soil and the mammalian skin and respiratory tract, respectively. In these environments, both organisms frequently encounter nitric oxide (NO), a key signaling molecule in both bacteria and eukaryotes (for review, see [20]). Indeed NO, which is toxic at high doses through the production of reactive nitrogen species (RNS), is produced primarily by denitrifying bacteria in the soil and by macrophages in the mammalian host, but some species, notably *Bacilli*, *Staphylococci* and *Streptomyces*, can also synthesize NO via bacterial NO synthases (bNOS) [21]. NO has been shown in a number of bacteria to provide protection from oxidative stress, provoked either by peroxide [22,23,24] or antibiotics [25,26]. The beneficial effects of NO can also be shared between bacteria and their hosts; NO produced by *B. subtilis* in the intestine of *C. elegans* has been shown to increase the lifespan of the nematode [27]. Despite its importance as both a signaling and potentially stress-inducing molecule, no bacterial sRNA that responds to NO levels has been identified to date. Given that *B. subtilis* is a non-pathogenic organism that occupies a very different niche to *S. aureus*, we were curious as to the physiological role and the targets of this sRNA in *B. subtilis*. We found that expression of RsaE, which we have renamed RoxS in *B. subtilis* for related to oxidative stress, is induced by NO in both *B. subtilis* and *S. aureus*. Despite their similarity in sequence and regulation in the two organisms, the genes affected by deletion of this sRNA are mostly different. Our data illustrate how the functions of a highly conserved sRNA have evolved in distantly related bacteria.

Results

RoxS expression is induced by the response regulator ResD in response to increased NO levels in *B. subtilis*

The chromosomal context of the *S. aureus* *rsaE* and *B. subtilis* *roxS* genes is very similar and, interestingly, many of the genes have functions related to redox homeostasis or show increased expression under conditions of diamide or peroxide-induced oxidative stress in *B. subtilis* (S1 Fig.) [28]. An alignment of the homologous *roxS/rsaE* genes from several *Bacilli* and *Staphylococci* showed significant sequence conservation in the promoter region (S2 Fig.). An examination of a conserved 8-nucleotide (nt) sequence around position -65 suggested that ResD, the response regulator of the two-component system (TCS) ResDE, that is sensitive to both O₂ and NO levels [29,30], might recognize this promoter region. Indeed, the sequence upstream of the *roxS* promoter is highly similar to the validated ResD binding site found upstream of the *yclJ* gene [31]. We therefore tested whether the expression of RoxS was altered in a mutant lacking the ResDE TCS. In mid-log phase, a ResDE deletion strain showed a three to four-fold decrease in RoxS expression and this effect was complemented by a plasmid expressing ResDE under IPTG control (Fig. 1B), indicating that ResD is an activator of RoxS transcription. The effect of the ResDE deletion was even stronger as the cells progressed towards stationary phase, confirming its importance as a regulator of RoxS expression (Fig. 1C). In agreement with our data, a recent chromatin immunoprecipitation study has shown a ResD binding at this location of the *B. subtilis* chromosome [32]. In contrast, the thiol specific

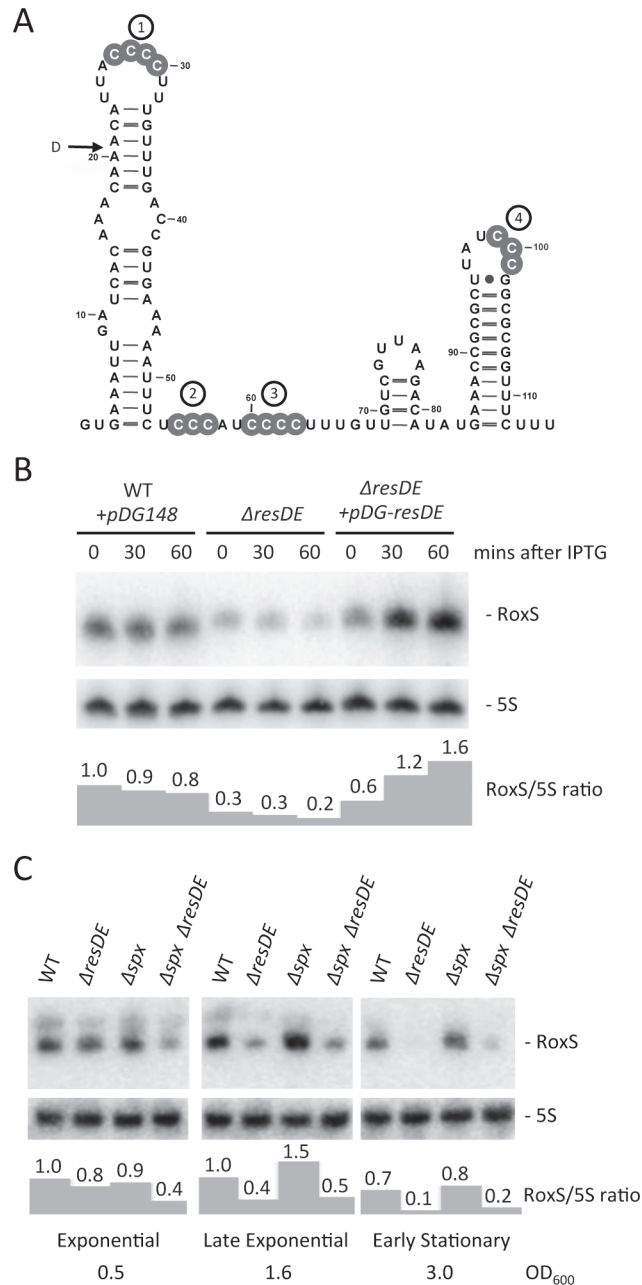


Figure 1. Regulation of RoxS expression by the ResDE two-component system. (A) Consensus secondary structure of RoxS generated with the help of LocARNA (<http://rna.informatik.uni-freiburg.de/LocARNA/>). Conserved groups of C-residues are shown in grey circles and are presented as numbered C-rich regions (CRR1-4). The 5' end of the degradation intermediate (D) observed in the $\Delta rnjA$ strain is indicated. (B) Northern blot showing RoxS expression in wild-type (WT), a $\Delta resDE$ mutant and a $\Delta resDE$ strain complemented with a plasmid expressing *resDE* under IPTG control. Strains used were CCB195 (WT + pDG148), CCB310 ($\Delta resDE$) and CCB503 ($\Delta resDE$ + pDG-resDE). Total RNA was isolated at different times after the addition of 1 mM IPTG to liquid cultures and the blot probed with oligo CC875 (S4 Table). 5S rRNA was probed as a loading control (oligo HP246). RoxS/5S ratios normalized to the WT strain at T0 are presented under the autoradiogram. (C) Northern blot showing RoxS expression in wild-type (WT), CCB310 ($\Delta resDE$), CCB628 (Δspx) and CCB629 ($\Delta resDE \Delta spx$) mutant strains in cells growing in rich medium in different growth phases. RoxS/5S ratios normalized to the WT strain in exponential phase (OD₆₀₀ = 0.5) are presented under the autoradiogram.

doi:10.1371/journal.pgen.1004957.g001

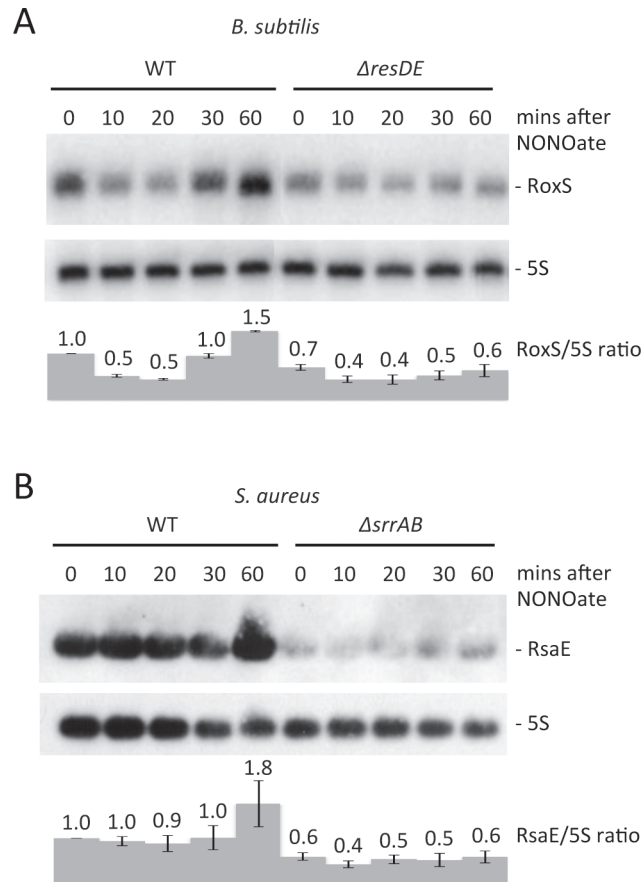


Figure 2. Nitric oxide dependent expression of RoxS in *B. subtilis* and *S. aureus*. Northern blots showing expression of RoxS in (A) wild type (WT) and CCB310 ($\Delta resDE$) *B. subtilis* cells and (B) wild type (WT; HG001) and HG001- $\Delta srrAB$ *S. aureus* cells at times after the addition of 100 μ M spermine NONOate to cultures growing in rich medium. 5S rRNA was probed as a loading control. RoxS/5S ratios normalized to the WT strain at T0 are presented under each autoradiogram, with standard errors as shown.

doi:10.1371/journal.pgen.1004957.g002

oxidative stress regulator Spx, also shown to bind in this region [33], had little effect on RoxS expression under the conditions tested.

The membrane-bound ResE sensor kinase responds to either decreased dissolved O₂ or increased NO levels [34] by a mechanism that is still not completely understood. It then activates the ResD response regulator through phosphorylation. We tested the effect of NO on RoxS expression by adding spermine NONOate to growing cultures. Spermine NONOate dissolves at neutral pH with a half-life of about 39 mins to produce NO. Expression of RoxS decreased slightly before increasing to a peak 30 mins to 1 h after addition of spermine NONOate (Fig. 2A). Although RoxS expression also decreased slightly upon addition of spermine NONOate to the $\Delta resDE$ mutant strain, no significant increase was observed after 1 h of incubation. Thus, the NO-dependent induction of RoxS expression depends on the ResDE TCS.

RsaE expression is also NO and ResDE/SrrAB-dependent in *S. aureus*

Given the strong conservation of the predicted ResD binding site upstream of RsaE in *Staphylococci*, we asked whether expression of RsaE was subjected to a similar regulation in *S. aureus*. The *S. aureus* homolog of the ResDE is called SrrAB and this TCS is also known to respond to low O₂ levels and NO [30]. The effect of NO on RsaE expression was also tested by adding

spermine NONOate under identical conditions to those described for *B. subtilis*. As for *B. subtilis* RoxS, we observed a weak but significant increase in RsaE expression about 1 h after the addition of spermine-NONOate to the growth medium in the wild-type (WT) strain (Fig. 2B). As anticipated, expression of RsaE was significantly lower in steady state conditions in the *srrAB* mutant, suggesting that SrrA is an activator of RsaE transcription. Furthermore, expression of RsaE was no longer induced by the addition of spermine-NONOate in this strain, clearly showing that the induction of RsaE by NO is dependent on the SrrAB TCS. Therefore, the signaling pathway and the expression of *S. aureus* RsaE and *B. subtilis* RoxS have been maintained during evolution.

B. subtilis strains lacking RoxS show increased expression of genes with redox-related functions

To get insight into the regulatory role(s) of RoxS in *B. subtilis*, we performed both proteome and transcriptome analysis in strains lacking RoxS. We detected 1092 proteins in whole cell extracts by LC-MS/MS and identified 63 proteins with significantly increased levels in the Δ roxS strain compared to the WT strain (≥ 1.5 -fold increase by two independent methods of analysis: Spectral Counting and MS1 Filtering; S1 Table). No proteins showed significantly decreased expression in the Δ roxS strain relative to WT. Nineteen of the up-regulated candidates (30%) had functions related to oxidation-reduction processes (Fig. 3), a significant enrichment from the 8.5% of *B. subtilis* genes associated with this Gene Ontology (GO) term (GO:0055114) genome-wide.

A number of the candidates showing increased expression in the Δ roxS strain (and therefore down-regulated by RoxS) are predicted to be involved in oxidative stress protection. These include the putative peroxiredoxins Tpx, AhpC and YgaF, and the thioredoxin-like protein YdbP. We also observed increased expression of the peptide methionine sulfoxide reductase MsrA, the DNA-protecting ferritin Dps and two heme-degrading mono-oxygenases HmoA and HmoB, all of which have been shown involved in resistance to oxidative stress in different *Bacilli* [35–37]. The increased expression of these proteins suggests that cells lacking RoxS are either experiencing, or behave as if they are experiencing oxidative stress, in conditions that are not normally stressful for WT cells.

Eleven of the proteins showing increased expression in the Δ roxS strain use prosthetic groups (NAD, FAD, FMN, heme, iron-sulfur clusters) for their oxido-reduction/electron transfer reactions (Fig. 3 and S1 Table). These include the short-chain flavodoxins YkuN and YkuP. YkuN has been shown to be capable of transporting electrons to *B. subtilis* nitric oxide synthase (bsNOS) to generate NO from arginine [38]. Interestingly, five of the proteins showing increased levels in the RoxS deletion mutant were members of the ferric uptake regulator (Fur) regulon, YkuN, YkuP, HmoA, YcgT and FeuA (iron hydroxamate binding lipoprotein), and four were members of the general stress sigma B (SigB) regulon, YdbP, Dps, YtkL (a predicted metal hydrolase) and SigB itself. One of the proteins that showed the greatest increase in expression levels was PpnKB, an inorganic polyphosphate/ATP-NAD kinase that converts NAD^+ to NADP^+ . Although this enzyme is not directly involved in a redox reaction, it does have an influence on the cell's levels of reducing power through the production of NADPH. The *ppnKB* mRNA is predicted to be a direct target for RoxS repression (see below).

The transcriptome analysis was performed using tiling arrays with 22 nt resolution as described previously [39]. A comparison of the RoxS deletion strain to the WT parental strain showed 46 mRNAs with increased expression levels and 48 with decreased synthesis (≥ 2 -fold; q -value < 0.05 ; S2 Table). Most (28/48) of the genes with decreased expression levels in the deletion strain were from the PBSX prophage, including all 12 members of the sigma factor Xpf

Proteome

Protein	$\Delta roxS$ /WT Spectral Counting	$\Delta roxS$ /WT MS1 Filtering	Biological Process	Binding	Regulon	Protein Description
YrkL	5.33	2.52	oxido-reduction	NADPH	-	Uncharacterized NAD(P)H oxidoreductase YrkL
PpnKB*	4.50	8.96	NADP biosynthesis	NAD/NADP	-	Probable inorganic polyphosphate/ATP-NAD kinase 2
YcgT	3.90	3.30	oxido-reduction	NADP	Fur	Ferredoxin--NADP reductase 1
YkhA*	3.56	2.63	metabolism	-	-	Uncharacterized acyl-CoA thioester hydrolase YkhA
YkuN	3.50	4.37	oxido-reduction	Fe/FMN	Fur/PerR	Probable flavodoxin-1
SigB	3.00	4.09	transcription	-	SigB	RNA polymerase sigma-B factor
YvaA/IolW	3.00	3.34	oxido-reduction	-	-	scyllo-inositol dehydrogenase
CitZ*	2.75	5.19	TCA cycle	-	CcpA	Citrate synthase 2
LplJ	1.71	2.49	protein lipoylation	-	-	lipoate-protein ligase
Dps	2.40	3.16	oxido-reduction	Fe	SigB	Ferritin/General stress protein 20U
YtkL	2.36	2.42	metabolism	-	SigB	UPF0173 metal-dependent hydrolase YtkL
YhfE	2.30	4.73	proteolysis	-	-	Putative aminopeptidase/endogluconase YhfE
NfrL	2.21	2.35	oxido-reduction	NADP/FMN	SigD	FMN reductase (NADPH)
FeuA	2.14	2.73	iron homeostasis	Fe	Fur	Iron-uptake system-binding protein
PyrK	2.13	2.29	oxido-reduction	2Fe-2S	PyrR	Dihydroorotate dehydrogenase B (NAD(+)), electron transfer subunit
SucD*	1.92	2.03	TCA cycle	-	-	Succinyl-CoA ligase [ADP-forming] subunit alpha
YkuP	1.89	2.41	oxido-reduction	Fe/FMN	Fur/PerR	Probable flavodoxin-2
Ahp	1.82	2.57	oxido-reduction	-	PerR	Alkyl hydroperoxide reductase subunit C
HmoB	1.81	2.71	oxido-reduction	heme	-	Heme-degrading monooxygenase HmoB
YktB	1.78	2.36	unknown	-	-	conserved hypothetical protein YktB
MsrA	1.76	2.76	oxido-reduction	-	-	Peptide methionine sulfoxide reductase MsrA
HmoA	1.62	2.87	oxido-reduction	heme	Fur	Heme-degrading monooxygenase HmoA
Tpx	1.61	1.76	oxido-reduction	-	-	Probable thiol peroxidase
CccB	1.60	2.05	oxido-reduction	heme	-	Cytochrome c-551
YdbP	1.58	2.01	oxido-reduction	-	SigB	Thioredoxin-like protein YdbP
YwrO	1.56	2.22	oxido-reduction	-	-	Nitroreductase/General stress protein 14
DefB	1.56	1.61	translation	Fe	-	Peptide deformylase 2
EtfA*	1.54	8.65	oxido-reduction	FAD	CcpA	Electron transfer flavoprotein subunit alpha
YueD	1.52	2.22	oxido-reduction	-	-	Benzyl reductase ((S)-benzoin forming)
YgaF	1.50	1.86	oxido-reduction	-	-	Putative peroxiredoxin YgaF

Transcriptome

Gene	$\Delta roxS$ /WT	q-value	Biological Process	Binding	Regulon	Protein Description
yvgN	4.70	0.00	oxido-reduction	NADP	-	Glyoxal reductase
ykuN	4.65	0.00	oxido-reduction	Fe/FMN	Fur/PerR	Probable flavodoxin-1
cydA	4.43	0.00	oxido-reduction	heme	ResD/Rex/CcpA	Cytochrome bd ubiquinol oxidase subunit 1
ykuO	4.22	0.00	unknown	-	Fur/PerR	conserved hypothetical protein
ykuP	3.34	0.01	oxido-reduction	Fe/FMN	Fur/PerR	Probable flavodoxin-2
ldh	3.03	0.01	oxido-reduction	NAD	ResD/Rex	L-lactate dehydrogenase
dhbE	2.84	0.00	siderophore biosyn.	-	Fur/PerR	2,3-dihydroxybenzoate-AMP ligase
yusI	2.84	0.00	oxido-reduction	-	-	putative oxidoreductase with thioredoxin domain
resA	2.62	0.00	oxido-reduction	-	PhoP/ResD	Thiol-disulfide oxidoreductase ResA
yxeB	2.45	0.01	iron homeostasis	Fe	Fur	Iron(3+)-hydroxamate-binding protein YxeB [Fe-ion]
tpx	2.45	0.01	oxido-reduction	-	-	Probable thiol peroxidase
yoxD	2.44	0.01	oxido-reduction	-	-	Uncharacterized oxidoreductase YoxD
dhbA	2.35	0.03	oxido-reduction	-	Fur/PerR	2,3-dihydro-2,3 dihydroxybenzoate dehydrogenase
dhbC	2.30	0.03	siderophore biosyn.	-	Fur/PerR	Isochorismate synthase DhbC
dhbB	2.18	0.05	siderophore biosyn.	-	Fur/PerR	Isochorismatase
yusV	2.18	0.01	iron homeostasis	Fe	Fur	Probable siderophore transport system ATP-binding protein [Fe-ion]
yktB	2.17	0.01	unknown	-	-	conserved hypothetical protein YktB
yhfE	2.14	0.01	proteolysis	-	-	Putative aminopeptidase/endogluconase YhfE
tkk	2.11	0.01	pentose phosphate	-	SpoOA	transketolase
dapB	2.08	0.01	oxido-reduction	NAD/NADP	-	4-hydroxy-tetrahydrodipicolinate reductase
lplJ/yhfJ	2.07	0.02	protein lipoylation	-	-	lipoate-protein ligase
gndA	2.03	0.01	oxido-reduction	NADP	-	6-phosphogluconate dehydrogenase, NADP(+)-dependent
rocA	2.02	0.03	oxido-reduction	-	AhrC/RocR	1-pyrroline-5-carboxylate dehydrogenase
rocG	2.01	0.02	oxido-reduction	NAD	RocR	Catabolic NAD-specific glutamate dehydrogenase RocG
catD	0.42	0.01	oxido-reduction	-	CatR/YodB	Putative oxidoreductase CatD
catE	0.41	0.00	oxido-reduction	Fe	CatR/YodB	Catechol-2,3-dioxygenase
yrdP/czcO	0.24	0.00	oxido-reduction	K/Co/Zn	-	Putative oxidoreductase CzcO

Figure 3. Selected candidates from proteome and transcriptome analyses of Δ roxS strain. Candidates found in both proteome and transcriptome are in bold type and highlighted in blue. Potential direct targets are marked with an asterisk and highlighted in beige (note for *sucD*, potential target is first gene in operon *sucC*). Candidates involved in oxido-reduction reactions are highlighted in violet. Candidates involved in oxidative stress protection are in red font. Members of the Fur and SigB regulons are highlighted in green and in pink, respectively.

doi:10.1371/journal.pgen.1004957.g003

regulon. Nine of the genes with augmented expression in the Δ roxS strain were members of the Fur regulon, consistent with the proteome data, although some of the genes concerned were different (Fig. 3). They include the *yxeB* and *yusV* genes, involved in the acquisition of iron, the *dhbABCE* operon involved in siderophore biosynthesis and the flavodoxin-encoding *ykuNOP* operon. YkuN and YkuP were among six candidates also identified in the proteome analysis, the others being Tpx, LplJ (lipoate protein ligase), YhfE (putative endogluconase) and YktB (unknown). We confirmed the increase in *ykuNOP* expression in the Δ roxS strain by Northern blot (S3A Fig.) although we suspect it may be an indirect consequence of the *roxS* deletion on Fur activity (see below). Furthermore, genes encoding a thioredoxin (*resA*) and the putative peroxiredoxin (*tpx*) also showed increased expression in the absence of RoxS. The *resA* gene encodes an extracytoplasmic thioredoxin involved in the maturation of cytochrome C, while the function of Tpx is still unknown. Two genes involved in the pentose phosphate pathway, *tkt*, encoding transketolase and *gndA*, encoding 6-phospho-gluconate dehydrogenase, also showed increased transcript levels. The pentose phosphate pathway is a major source of NADPH production in the cell for use as a reducing agent in anabolic reactions such as lipid and nucleic acid synthesis. Overall, fourteen of the up-regulated genes in the tiling array (30%) had annotated functions related to oxidation-reduction reactions (GO term 0055114), consistent with the functional enrichment seen in the proteome study (Fig. 3 and S2 Table). These data are in good agreement with a general role for RoxS in the redox state/oxidative stress response.

RoxS inhibits initiation of *ppnKB* mRNA translation

Because most sRNAs base-pair to mRNA targets, we used several programs (TargetRNA2 [40], CopraRNA [41], RNApredator [42]) to predict potential direct mRNA targets of RoxS, with a particular focus on the translation initiation region. The targets suggested by CopraRNA were highly enriched for mRNAs involved in a relatively small number of cellular processes including electron transport, respiration, lipid metabolism and metal binding (S4 Fig.). The best target proposed by TargetRNA2 and RNA predator, the *ppnKB* mRNA (Fig. 4A), was consistent with this functional enrichment. Furthermore, the synthesis of the PpnKB protein was 4.5 to 9-fold increased in the Δ roxS strain by Spectral Counting and MS1 Filtering, respectively (Fig. 3). We therefore chose to study the RoxS-dependent regulation of *ppnKB* in more detail.

To determine whether RoxS could directly bind to the *ppnKB* mRNA to inhibit translation initiation, we tested the effect of RoxS on the formation of the ribosomal initiation complex on the *ppnKB* mRNA by toeprinting assays. Addition of 30S ribosomal subunits and initiator tRNA to the *ppnKB* transcript, showed a clear toeprint at position +16 relative to the *ppnKB* start codon (Fig. 4B; lane 5). Incubation of the *ppnKB* transcript with equimolar and higher concentrations of RoxS resulted in complete inhibition of the 30S ribosome toeprint, while a band specific to the binding of RoxS appeared at position -9/10 (Fig. 4B; lane 6 and 7). In contrast, RoxS had a much weaker effect on the formation of the initiation complex on the *ykuN* transcript (S3B Fig.) and did not show evidence for a stable interaction around the SD sequence, consistent with the fact that, despite the presence of four consecutive G-residues in the SD, it was not predicted as a target by any of the three algorithms (including the ORFs, for TargetRNA2). This experiment shows that RoxS specifically binds to the *ppnKB* mRNA and forms a stable complex that is sufficient to prevent the formation of the ternary translation initiation

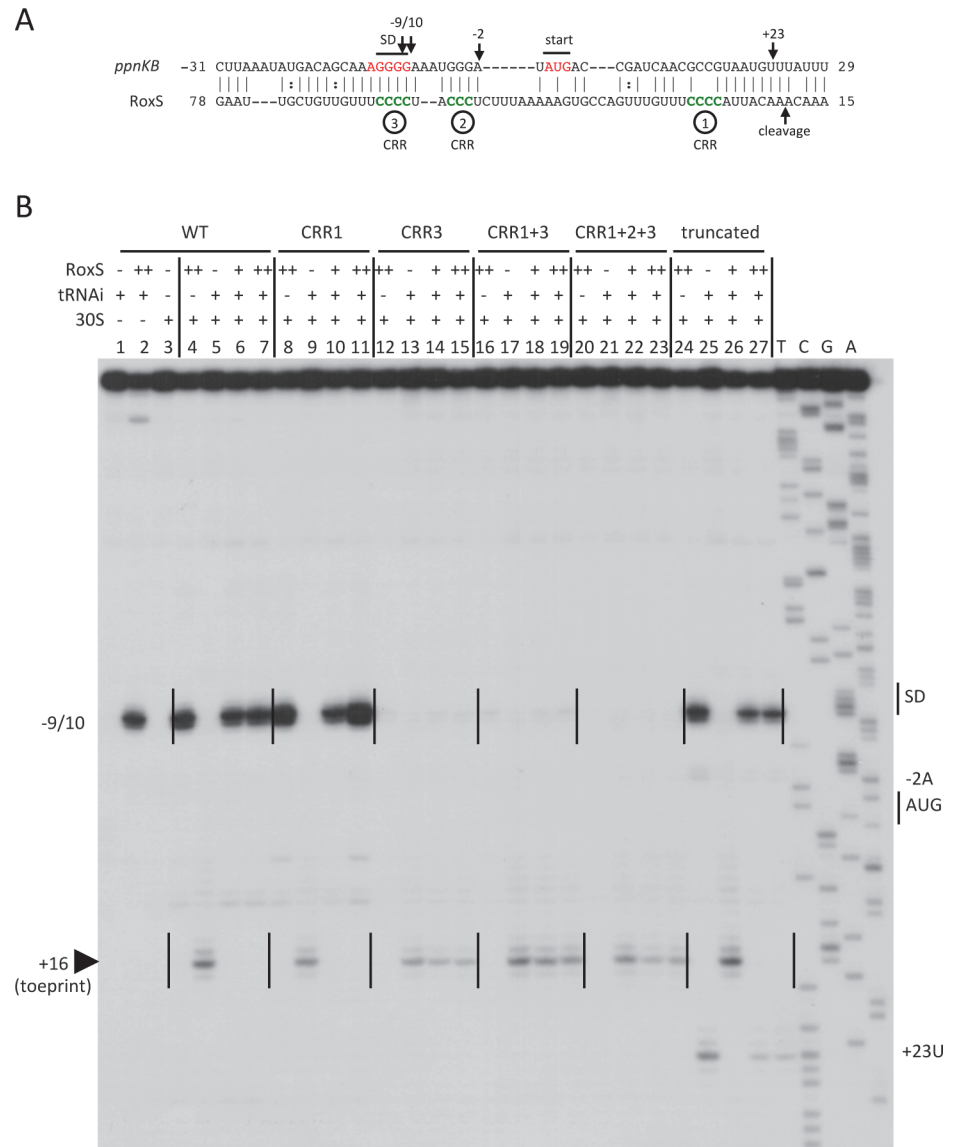


Figure 4. Inhibition of translation initiation complex formation on the *ppnKB* mRNA by RoxS. (A) Predicted base-pairing interactions between RoxS and the *ppnKB* mRNA by TargetRNA2 (<http://cs.wellesley.edu/~btjaden/TargetRNA2/>). The CRR regions 1–3 are shown in green. In the mutant forms, the four cytosine residues of CRR1 and CRR3 have been replaced by adenines and the three cytosines of CRR2 replaced by a GAA sequence. The Shine and Dalgarno (SD) sequence and AUG initiation codon (start) are indicated in red. The site of reverse transcriptase stops (–9/10, –2, +23) in the toeprint assay with full-length and truncated forms of RoxS are indicated by vertical arrows. The mapped RNase Y cleavage site in RoxS is indicated. (B) Toeprint analysis of full-length (WT) and various mutant or truncated forms of RoxS bound to the *ppnKB* mRNA. The toeprint formed by the 30S ribosomal subunit is indicated at +16 relative to the first nt of the start codon (AUG). Efficient binding of RoxS to *ppnKB* is characterized by a strong RT stop at nts –9/10. Additional RT stops observed only with the truncated form of RoxS are indicated at positions –2 and +23. The Shine and Dalgarno sequence is indicated by SD. (++) indicates addition of twice the quantity of RoxS (80 nM vs. 40 nM) as in lanes marked with (+).

doi:10.1371/journal.pgen.1004957.g004

complex. The toeprinting assays, coupled with the fact that RoxS is not predicted to make significant interactions with any portion of the *ykuNOP* mRNA, suggest that RoxS-dependent effect on the expression this operon, observed in both the transcriptome and proteome analysis, most likely results from an indirect effect.

C-rich region 3 is key for RoxS binding to the *ppnKB* mRNA and inhibiting translation initiation complex formation

The base-pairing interaction between RoxS and *ppnKB* predicted by TargetRNA is extensive (Fig. 4A) and includes the first three C-rich regions (CRR1-3). However, the strong reverse transcriptase (RT) stop at nt -9/10 provoked by duplex formation is close to the SD sequence, suggesting the most stable interaction is between CRR3 and the *ppnKB* ribosome binding site. However, the six nts downstream of CRR1 are identical to those downstream of CRR3, creating a 10 nt duplication (CCCCUUUGUU) in RoxS and leaving open the possibility that the two sequences were functionally redundant. We therefore performed toeprinting assays with RoxS variants where the four consecutive C-residues of CRR1 or CRR3, or both, were changed to A. These mutations are not predicted to alter the secondary structure of RoxS.

The data clearly showed that mutation of CRR3 alone abolished the ability of RoxS to bind the mRNA and to inhibit 30S ribosome binding to *ppnKB* (Fig. 4B, lanes 14–15). Conversely, mutation of CRR1 alone had no effect (Fig. 4B, lanes 10–11). RoxS mutants lacking both CRR1 and CRR3, or the three CRR's 1, 2 and 3, behaved similarly to the CRR3 mutant in failing to interact with the *ppnKB* mRNA or to inhibit translation initiation complex formation (Fig. 4B, lanes 18–19 and 22–23). Hence, these data show that CRR3 plays the most important role in inhibition of translation initiation and that the two repeat motifs of RoxS are not functionally equivalent for the regulation of *ppnKB*.

RoxS overexpression leads to degradation of the *ppnKB* mRNA

Binding of sRNAs can have direct effects on target mRNA stability, by creating new sites for endoribonuclease cleavage, or indirect effects through the increased exposure of existing cleavage sites following translational repression. We therefore asked whether overexpression of RoxS would lead to degradation of the *ppnKB* mRNA. For these studies, we used the Δ roxS mutant strain transformed with a plasmid expressing RoxS from a tetracycline-dependent promoter (strain CCB498: Δ roxS + pDG-Ptet-roxS) or with a control plasmid (strain CCB505: Δ roxS + pDG-Ptet). Induction of RoxS expression with increasing concentrations of anhydrotetracycline (aTc) in strain CCB498 caused a gradual reduction (about two-fold) in *ppnKB* mRNA levels compared to the empty vector control strain (Fig. 5), showing that RoxS affects the amount of *ppnKB* mRNA in the cell, in addition to controlling its translation.

Expression of RoxS from the pDG-Ptet vector is transient, reaching a peak about 5 mins after addition of aTc before decreasing rapidly (Fig. 6A, D), presumably due to an accumulation of the TetR repressor driven by the same promoter. We exploited this property of the plasmid to analyze whether *ppnKB* mRNA levels would recover upon shut-down of RoxS expression. Indeed, *ppnKB* mRNA levels fell to a minimum about 5 mins after induction of RoxS and were rapidly restored as RoxS levels decreased (Fig. 6A, D). The RoxS-dependent reduction in *ppnKB* levels was only slightly less efficient in a strain lacking the double-strand specific endonuclease RNase III, encoded by the *rnc* gene (Fig. 6B, D). However, it was significantly reduced in a strain lacking the single-strand specific nuclease RNase Y, encoded by *rny* (Figs. 6C, D). These results suggest that RNase Y is a key enzyme for RoxS-mediated *ppnKB* mRNA turnover, while RNase III plays a secondary role under these experimental conditions. It should be noted that RoxS is slow to shut-off in the *rny* mutant (Fig. 6C, D); we will see later that this is due to an effect of RNase Y on RoxS RNA stability.

To further show that RoxS controls *ppnKB* expression at the level of mRNA stability, we measured the half-life of the *ppnKB* mRNA in WT strains and mutant strains lacking either RNase III or RNase Y under steady state conditions (Fig. 7). The *ppnKB* mRNA was stabilized about 1.8-fold in cells lacking RoxS (8.4 vs. 15 mins half life, respectively in WT and Δ roxS

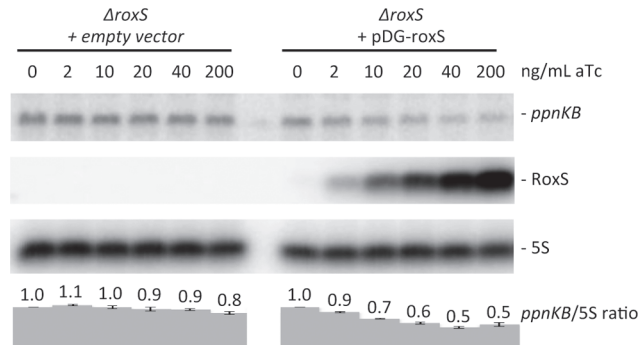


Figure 5. Induction of RoxS leads to decreased *ppnKB* mRNA levels. Northern blot showing decreased *ppnKB* mRNA levels upon RoxS induction. Total RNA was isolated 10 mins after addition of aTc to liquid cultures at concentrations shown and the blot was probed with oligo CC964 (S4 Table). Strains used were CCB505 (ΔroxS + empty vector) and CCB498 (ΔroxS + pDG-Ptet-roxS). 5S rRNA was probed as a loading control. *ppnKB*/5S ratios normalized to the condition without aTc are presented under the autoradiogram, with standard errors as shown.

doi:10.1371/journal.pgen.1004957.g005

strains), consistent with a role for RoxS in controlling *ppnKB* mRNA stability (Fig. 7A). In the absence of RNase III, a similar increase in *ppnKB* stability was seen, but was not further amplified by the additional deletion of *roxS* (Fig. 7B). The simplest explanation is that RNase III and RoxS collaborate to degrade a portion of *ppnKB* transcripts; the lack of either component, or both, leading to a similar increase in *ppnKB* mRNA stability.

The *ppnKB* mRNA was also significantly stabilized (8.4 vs. 24 mins) in the Δrny mutant compared to the WT strain (Fig. 7C), consistent with a role for RNase Y initiating the degradation of the *ppnKB* mRNA. In this case, however, further deletion of *roxS* had an additional stabilizing effect (24 vs. >40 mins half life, respectively). This suggests the existence of a RoxS-mediated *ppnKB* turnover pathway that is independent of RNase Y and that inactivation of both pathways are required for maximal stabilization of *ppnKB*. We propose that the second pathway is the RoxS/RNase III dependent pathway described above. The data also indicate an effect of RNase Y that is independent of RoxS (15 mins vs. >40 mins half-life, respectively, in ΔroxS vs. Δrny ΔroxS strains), consistent with a role for RNase Y in the non-regulated turnover of the *ppnKB* mRNA.

Interestingly, the *ppnKB* mRNA was highly unstable in a strain lacking the 5'-3' exoribonuclease RNase J1 (Fig. 7D) and this destabilization was attenuated upon deleting RoxS (3.1 vs. 9.4 mins half-life, respectively, in ΔrnjA vs. ΔrnjA ΔroxS strains). Data presented in the next section will shed light on this phenomenon. Globally, our data provide an illustration of the complex interplay between ribonucleases involved in the turnover of the *ppnKB* mRNA, both dependent and independent of RoxS-mediated repression.

Evidence for two pathways of RoxS turnover

We also analyzed the importance of the three main ribonucleases in the degradation of the RoxS sRNA. The half-life of the chromosomal copy of RoxS was first measured in WT cells and in cells lacking either RNase III, RNase Y or RNase J1. In WT cells and in cells lacking RNase III, RoxS showed bi-phasic RNA degradation upon transcription arrest with rifampicin (Fig. 8A, C), suggesting that two populations of this sRNA exist *in vivo*. The simplest interpretation is that these populations represent free RoxS or RoxS bound to its targets. While the half-life of the rapidly decaying population was similar in both strains, the slowly decaying population was strongly stabilized in the Δrnc mutant (Fig. 8C). Because of its specificity for

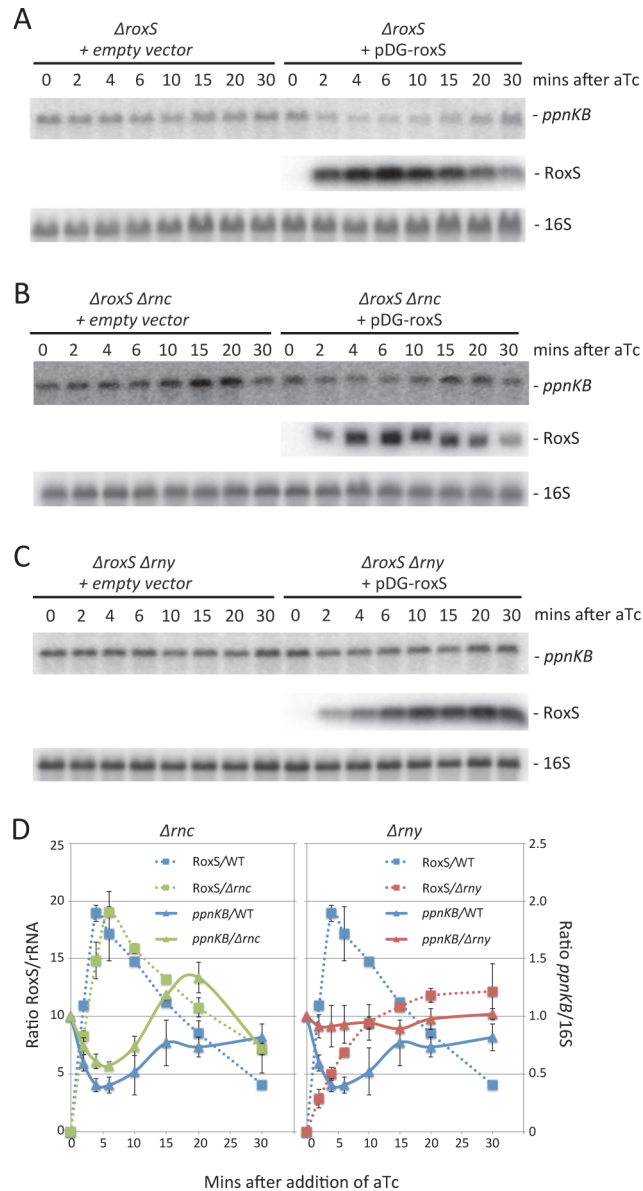


Figure 6. The reduction in *ppnKB* mRNA levels upon induction of RoxS expression is reversible and depends primarily on RNase Y. (A) Northern of total RNA isolated from strain CCB505 (*ΔroxS* + empty vector) and CCB498 (*ΔroxS* + pDG-Ptet-roxS) at times after the addition of 40 μg/mL aTc. The blot was re-probed for 16S rRNA (oligo CC058; S4 Table) as a loading control. (B) Same as panel A using RNase III mutant strains CCB530 (*ΔroxS Δrnc* + empty vector) and CCB531 (*ΔroxS Δrnc* + pDG-Ptet-roxS). (C) Same as panel A using RNase Y mutant strains CCB535 (*ΔroxS Δrny* + empty vector) and CCB533 (*ΔroxS Δrny* + pDG-Ptet-roxS). The RNAs isolated from strains CCB498, CCB531 and CCB533 in panels A, B and C were also run on a polyacrylamide gel and probed for RoxS. (D) Quantification of RoxS and *ppnKB* in Northern blots of strains containing pDG-Ptet-roxS. Left: WT and *Δrnc* backgrounds; Right: WT and *Δrny* backgrounds. The WT traces are the average of three experiments, and the *Δrnc* and *Δrny* traces are the average of two experiments, with standard errors as shown. *ppnKB* mRNAs were normalized to 16S rRNA and to the T0 sample (right hand Y-axis). RoxS was normalized to either 16S or 5S rRNA (left hand Y-axis).

doi:10.1371/journal.pgen.1004957.g006

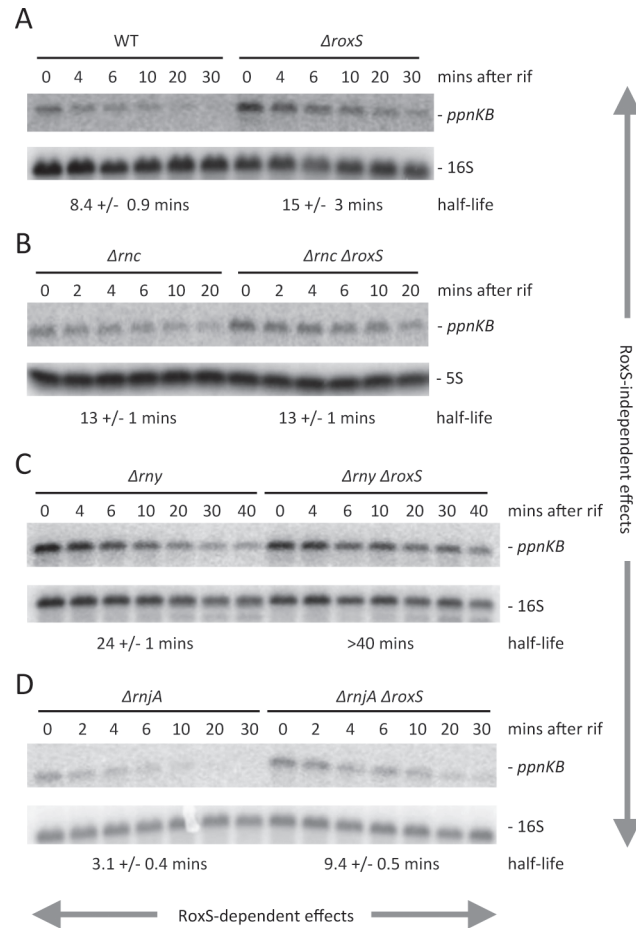


Figure 7. The stability of the *ppnKB* mRNA depends on RoxS, RNase III and RNase Y. (A) Northern blots of total RNA isolated from wild-type (WT) and Δ roxS strains (strain CCB485) probed for the *ppnKB* mRNA at times after addition of rifampicin (Rif) at 150 μ g/mL. The blot was re-probed for 16S rRNA for normalization. Calculated half-lives are shown beneath the autoradiographs and are the average of 2 to 4 experiments, with standard errors as shown. (B) Same as in panel A using RNase III mutant strains CCB418 (Δ rnc) and CCB515 (Δ rnc Δ roxS). (C) Same as in panel A using RNase Y mutant strains CCB441 (Δ rny) and CC558 (Δ rny Δ roxS). (D) Same as in panel A using strains CCB434 (Δ rnjA) and CCB559 (Δ rnjA Δ roxS). RoxS-dependent effects of the different RNases are indicated by horizontal arrows and RoxS-independent effects of the different RNases by vertical arrows.

doi:10.1371/journal.pgen.1004957.g007

double-stranded RNA, it is most likely that the stabilisation of the slowly decaying phase represents stabilisation of RoxS molecules that are hybridized to its mRNA targets. In cells lacking RNase J1 (Δ rnjA), full length RoxS was stabilized compared to the WT strain, but in addition a very long-lived degradation/processing intermediate was detected (Fig. 8B, C). This intermediate was not detected in the absence of RNase Y and the full-length RoxS had a much longer half-life in the Δ rny mutant strain (Fig. 8B, C). Using primer extension, we mapped the 5' end of the short RoxS fragment to nt +20 of RoxS (S5 Fig.). Together these results suggest that RNase Y initiates RoxS turnover by cleaving around nt +20 (Fig. 1) and RNase J1 degrades the downstream cleavage product, in addition to having some activity on the full-length RNA.

Because a small amount of RNase Y-cleaved RoxS was visible in WT cells (Fig. 8A), we asked whether this truncated form was functional and might contribute to regulation. We cloned a 5' truncated version of RoxS beginning at nt 20, called RoxS(Y), into the plasmid vector pDG-Ptet. In a manner similar to full-length RoxS, aTc induction of RoxS(Y) resulted in a

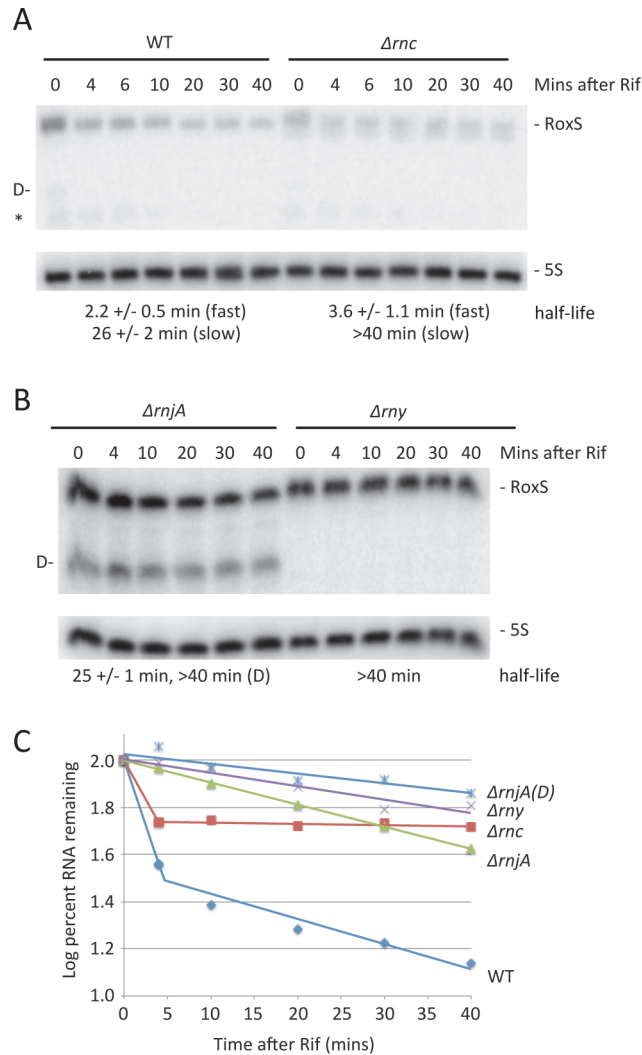


Figure 8. Two pathways of RoxS RNA turnover. (A) Northern blot of total RNA isolated at times after the addition of rifampicin (Rif) probed for RoxS in wild-type (WT) and Δrnc cells (strain CCB418). Membranes were re-probed for 5S rRNA for normalization. Half-lives are given under each blot, with standard errors as shown. In strains that have bi-phasic RNA degradation curves (see text), separate half-lives are given for the fast and slow phases of decay. The cleaved form of RoxS is labeled D on the left side of the autoradiogram. The origin of the species labeled with an asterisk is unknown. (B) Same as in panel A using strains CCB434 ($\Delta rnjA$) and CCB441 (Δrny). (C) Graph of representative RNA decay curves showing the log percent RNA remaining versus time after rifampicin addition.

doi:10.1371/journal.pgen.1004957.g008

rapid and efficient reduction in *ppnKB* levels, which then recovered as RoxS(Y) levels fell (S6A-S6B Fig.). Thus the truncated form of RoxS that accumulates in an RNase J1 mutant is fully functional and may explain the RoxS-dependent destabilization of *ppnKB* in the absence of RNase J1 (Fig. 7D). When tested in the toeprinting assay, the truncated RoxS species formed a more extensive hybrid than the full-length sRNA with the *ppnKB* mRNA, indicated by additional reverse transcriptase stops around nt -2 and nt +23 (Fig. 4B, lane 24). The short form was equally efficient as the full-length RoxS in inhibiting *ppnKB* translation initiation complex formation at the concentrations tested.

RoxS forms a duplex with the ribosome binding site of *ppnKB* mRNA and creates RNase III cleavage site

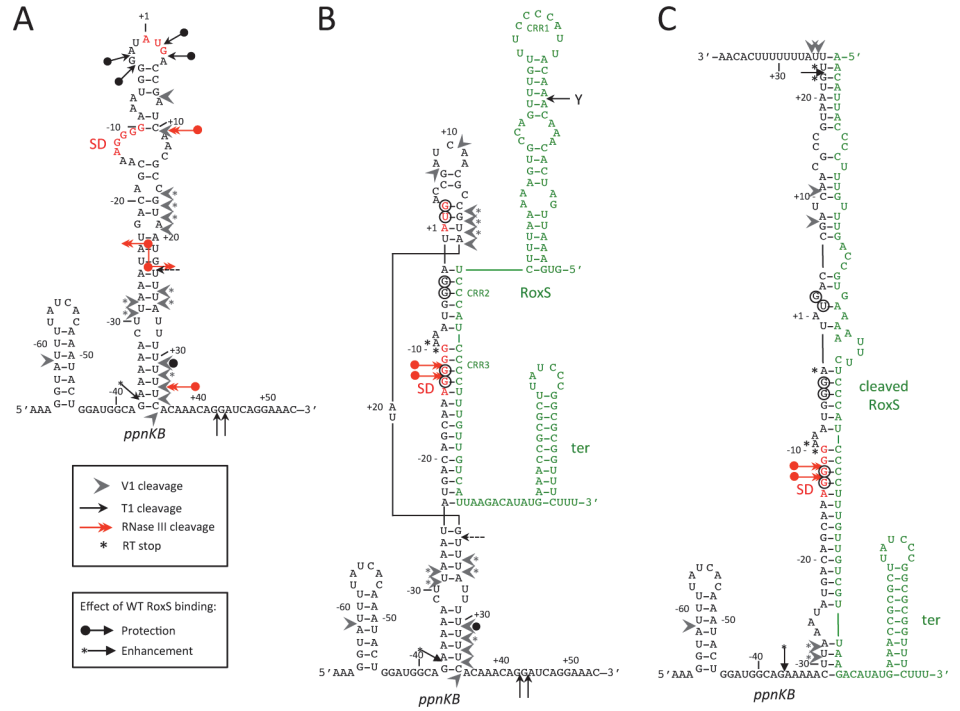
To characterize the interactions between *ppnKB* and RoxS and its various mutant forms, we performed structure probing experiments on the *ppnKB* mRNA using the double-strand-specific enzymes RNase V1 and RNase III, and RNase T1, which cleaves principally 3' to unpaired guanines (Fig. 9 and S7 Fig.). The data suggested that in the absence of RoxS, the *ppnKB* mRNA folds into a long, but relatively unstable hairpin structure that extends from nt -37 to nt +34 relative to the translation initiation site (Fig. 9A). Indeed, two major RNase T1 cleavages occur 3' to G-3 and G-4 and two lesser cleavages 3' to nts +2/+3 in the apical loop containing the AUG initiation codon while a number of RNase V1 cleavages are located in the irregular helix (Fig. 9A and S7A-S7B Fig.; lane 2). Consistent with this model, RNase III cleaves the large irregular helix of *ppnKB* at four sites (nts -24, +10, +22 and +32), with the cleavages at -24 and +22 producing the two-nt 3' overhang characteristic of RNase III processing (Fig. 9A and 9D; lane 3).

Binding of RoxS induces strong protection of the RNase T1 cleavages in the apical loop (G+3, G-3, G-4) and at G-12 and G-13 of the SD sequence while the cleavage at G-37 is slightly enhanced (Fig. 9B and S7A Fig.; lanes 3, 4). Concomitantly, RNase V1 cleavages are slightly enhanced at nts -29/30, +16 to +18, +24/25 and +31 (Fig. 9B and S7B Fig.; lanes 3, 4). Remarkably, all four RNase III cleavage sites are significantly reduced upon binding to RoxS while two strong adjacent cleavages appear in the *ppnKB* SD sequence at nts -12/13 (Fig. 9D; lanes 4, 5). These data suggest that the large hairpin loop of *ppnKB* undergoes a partial melting to promote basepairing interactions with RoxS, leading to the sequestration of the SD sequence. Identical changes in the RNase III cleavage patterns were observed if complex formation was performed with the truncated RoxS(Y) (Fig. 9C and 9D, lanes 22–25) or with the CRR1 mutant (Fig. 9D; lanes 6–9). However, RoxS derivatives with a mutation in CRR3 had no effect on the RNase III cleavages, showing that the mutated RNAs fail to interact with *ppnKB* (Fig. 9D). Identical conclusions were reached in the probing experiments with RNases T1 and V1 (S7 Fig.).

The proposed models for the interaction of *ppnKB* with full-length or truncated RoxS (Fig. 9B and C) take into account most of the data although we cannot completely distinguish between RoxS-dependent changes that are due to the formation of an extended RoxS/*ppnKB* duplex or due to a stabilization of existing *ppnKB* helices upon RoxS binding. However, the data unambiguously show that the CCR3 motif is responsible for the interaction with the SD sequence to prevent the formation of the translation initiation complex and to create a novel site for RNase III binding and cleavage.

The *sucCD* operon mRNA is a direct target of the cleaved form of RoxS

TargetRNA2 and CopraRNA both predicted the *sucC* gene, the first cistron of the *sucCD* operon encoding the two subunits of succinyl-coA synthase, as another potential target of RoxS (Fig. 10A). Differential proteomic analysis showed a 2-fold increased expression of SucD in the mutant Δ roxS strain, while SucC narrowly missed the dual 1.5-fold cut-off (1.4 fold increase by spectral counting; 1.8 fold increase by MS filtering) (Fig. 3, S1 Table). Interestingly, the *sucCD* mRNA was also shown to be a target of RsaE in *S. aureus* [17,18]. We therefore probed the membranes shown in Fig. 6 for the *sucCD* mRNA to see whether its mRNA levels were affected by RoxS expression. Transient expression of RoxS by aTc addition led to a similar decrease in *sucCD* expression as was observed for *ppnKB* (Fig. 10B, E). This decrease in expression was slightly attenuated in the absence of both RNase III (Fig. 10C, E) and RNase Y (Fig. 10D, E), suggesting roles for both of these enzymes in the turnover of the *sucCD* mRNA in response to RoxS expression.



D

	WT				CRR1			CRR3			CRR1,3			CRR1,2,3 truncated					T	C	G	A							
RoxS	++	-	++	++	++	-	++	++	++	-	++	++	++	-	++	++	++	-	++	++	++	-	++	++					
RNase III	-	+	+	+	-	+	+	+	-	+	+	+	-	+	+	+	-	+	+	+	-	+	+	+					
	1	2	3	4	5	6	7	8	9	10	11	12	13	14	15	16	17	18	19	20	21	22	23	24	25				

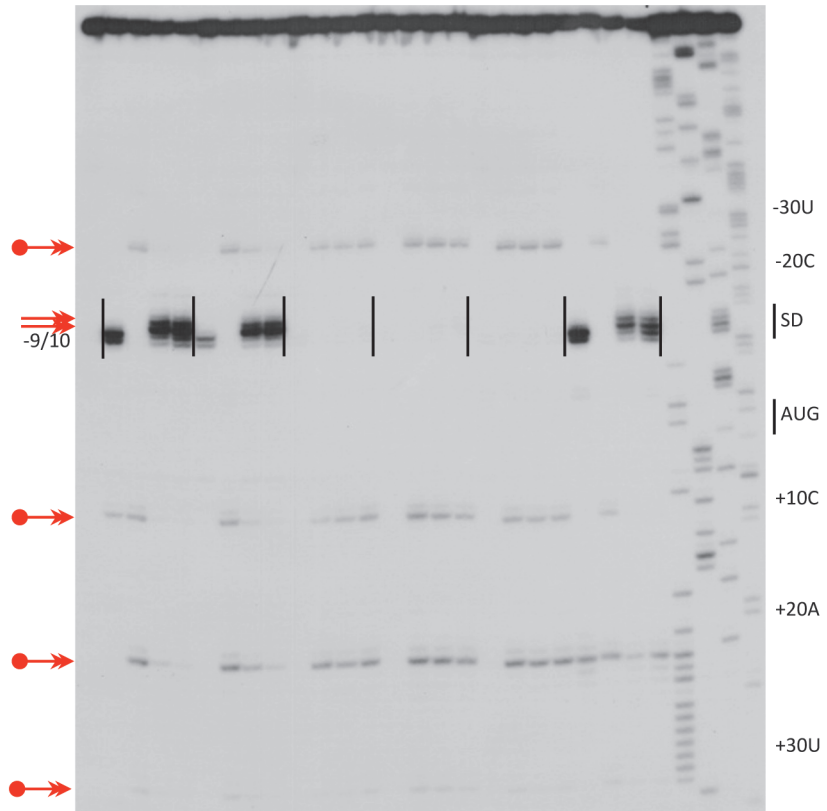


Figure 9. RNase III cleaves the *ppnKB*/RoxS duplex *in vitro*. (A) Summary of structure probing experiments showing proposed secondary structure around the translation initiation site of the *ppnKB* mRNA. The Shine and Dalgarno (SD) sequence is shown in red. The legend for the different cleavages is given under the schematic. (B) A proposed duplex formed between *ppnKB* (black) and full-length RoxS (green). The *ppnKB* Shine and Dalgarno sequence is shown in red. The legend for the different cleavages is the same as panel A. The CRR regions 1–3 of RoxS are indicated. The sites of protection from RNase T1 cleavages at –12/13, –3/4, and +2/3 upon duplex formation are encircled (S7 Fig). RoxS induced RT stops are marked with an asterisk. (C) Proposed duplex formed between *ppnKB* (black) and truncated RoxS (green). Legend as in panel B. (D) Autoradiograph of *in vitro* RNase III cleavage assays showing sites of RNase III cleavage (double-headed red arrows) in *ppnKB* bound to full-length (WT) or various mutant or truncated forms of RoxS. The 5' ends of primer extension products resulting from RNase III cleavage of *ppnKB* alone are identified to the right of the gel relative to the first nt of the AUG start codon (double-headed red arrows with circle). Note that cleavage sites are by convention identified by the nt immediately upstream of the corresponding primer extension product. The RT stops at positions –9/10 provoked by RoxS binding to *ppnKB* and the new RNase III cleavages at positions –12/13, seen upon duplex formation, are indicated to the left of the gel (double-headed red arrows). The Shine and Dalgarno sequence is indicated by SD. (++) indicates addition of twice the quantity of RoxS (80 nM vs. 40 nM) as in lanes marked with (+).

doi:10.1371/journal.pgen.1004957.g009

We then analyzed the effect of RoxS and its variants on the formation of the translation initiation complex formed with the *sucC* mRNA using toeprinting assays. In contrast to the *ppnKB* mRNA, RoxS binding did not prevent the formation of the initiation complex on *sucC*, even at the highest RoxS concentration (Fig. 11, lanes 6 and 7). Only a weak RT pause characteristic of RoxS binding was observed at nt +4/5 relative to the first nt of the open reading frame, indicating that RoxS did not form a stable complex with *sucC* (Fig. 11, lane 4). To our surprise, the truncated form of RoxS(Y) bound far more efficiently than RoxS to the *sucCD* mRNA, causing a very strong RT pause at position –2/–3 and an increased signal at +4/5 (Fig. 11, lane 24). As a consequence, this led to a strong and efficient inhibition of the toeprint at +16 by the truncated form of RoxS (Fig. 11, lanes 26 and 27) comparable to that seen with *ppnKB* (Fig. 4, lanes 6 and 7). This experiment suggests that processing of RoxS is necessary for regulation of *sucC* and that truncation at the 5' end of RoxS expands the repertoire of effective targets for this sRNA.

Discussion

The RoxS sRNA belongs to the ResD regulon and regulates the response to NO

In this paper, we have shown that expression of the regulatory RNA RoxS/RsaE is induced by nitric oxide in both *B. subtilis* and *S. aureus*, in a mechanism that is dependent on their respective orthologous two-component systems, ResDE and SrrAB. The membrane-bound sensor protein ResE/SrrB is autophosphorylated in response to both NO and limiting O₂ levels, and in turn phosphorylates the response regulator ResD (SrrA in *S. aureus*) [31,43]. NO and hypoxia inhibit terminal oxidases and limit the flow of electrons through the electron transport chain. It was recently suggested that the resulting accumulation of reduced menaquinones in the membrane is likely to be the trigger that activates the ResDE/SrrAB TCS [30], similar to the quinone-sensitive ArcAB TCS in *E. coli* [44]. In *S. aureus*, SrrAB is important for cell survival in the host environment and in biofilms. This system senses and responds to both NO and hypoxia, and regulates genes required for cytochrome biosynthesis and assembly, anaerobic metabolism, iron-cluster repair, and NO detoxification [43]. In *B. subtilis*, ResD is known to activate the expression of about 30 genes involved in the anaerobic respiration of nitrate, the production of cytochromes, the fermentation of pyruvate and in NO detoxification [45].

Here, we have studied in more detail the regulatory functions of *B. subtilis* RoxS, which further expands the regulatory impact of ResD. Interestingly, regulation by ResD is significantly

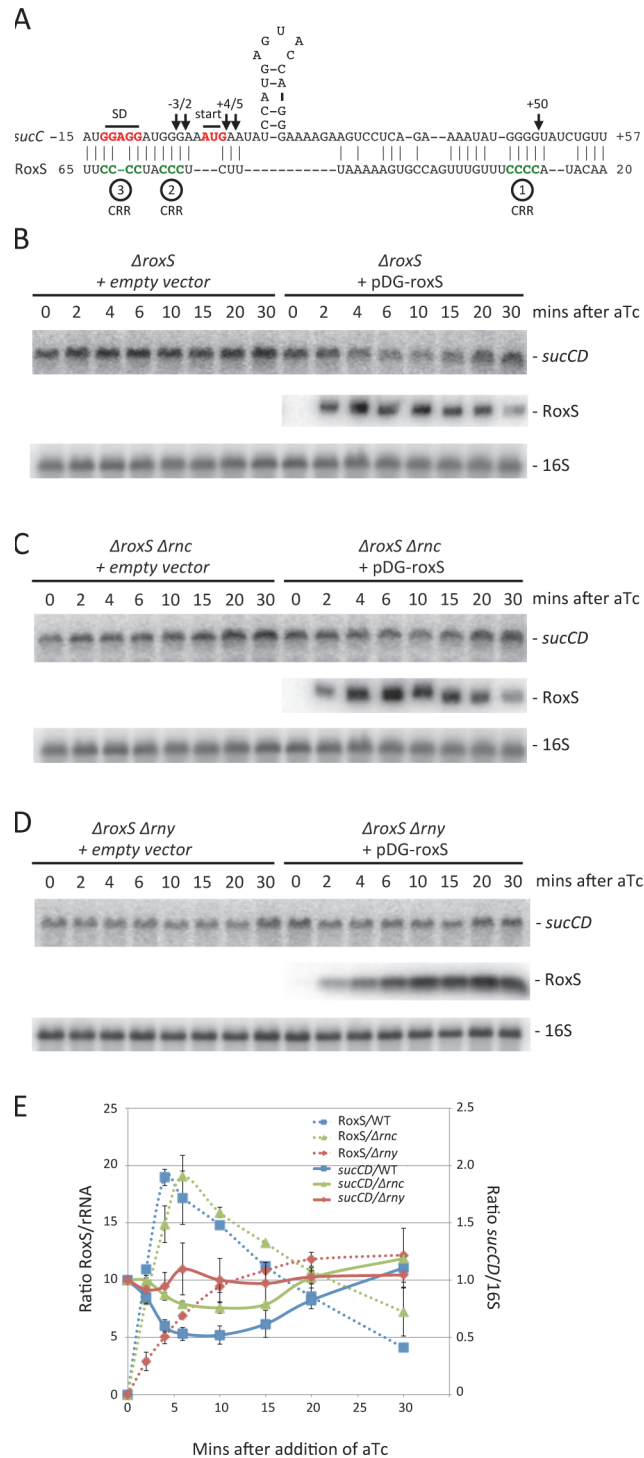


Figure 10. Targeted degradation of the *sucCD* mRNA upon induction of RoxS expression. (A) Predicted base pairing between RoxS and the *sucCD* mRNA by TargetRNA2 (<http://cs.wellesley.edu/~btjaden/TargetRNA2/>). The CRR regions 2 and 3 of RoxS are shown in green. The Shine Dalgarno (SD) sequence and AUG initiation codon (start) of *sucC* are indicated in red. (B), (C), (D) Northern blots from Fig. 5 reprobed for the *sucCD* mRNA with an oligo specific for the *sucD* portion of the bicistronic transcript (CC1408; S4 Table). (E) Quantification of RoxS and *sucCD* in Northern of strains containing pDG-Ptet-roxS. Legend as in Fig. 5D. The traces are the average of two experiments, with standard errors as shown.

doi:10.1371/journal.pgen.1004957.g010

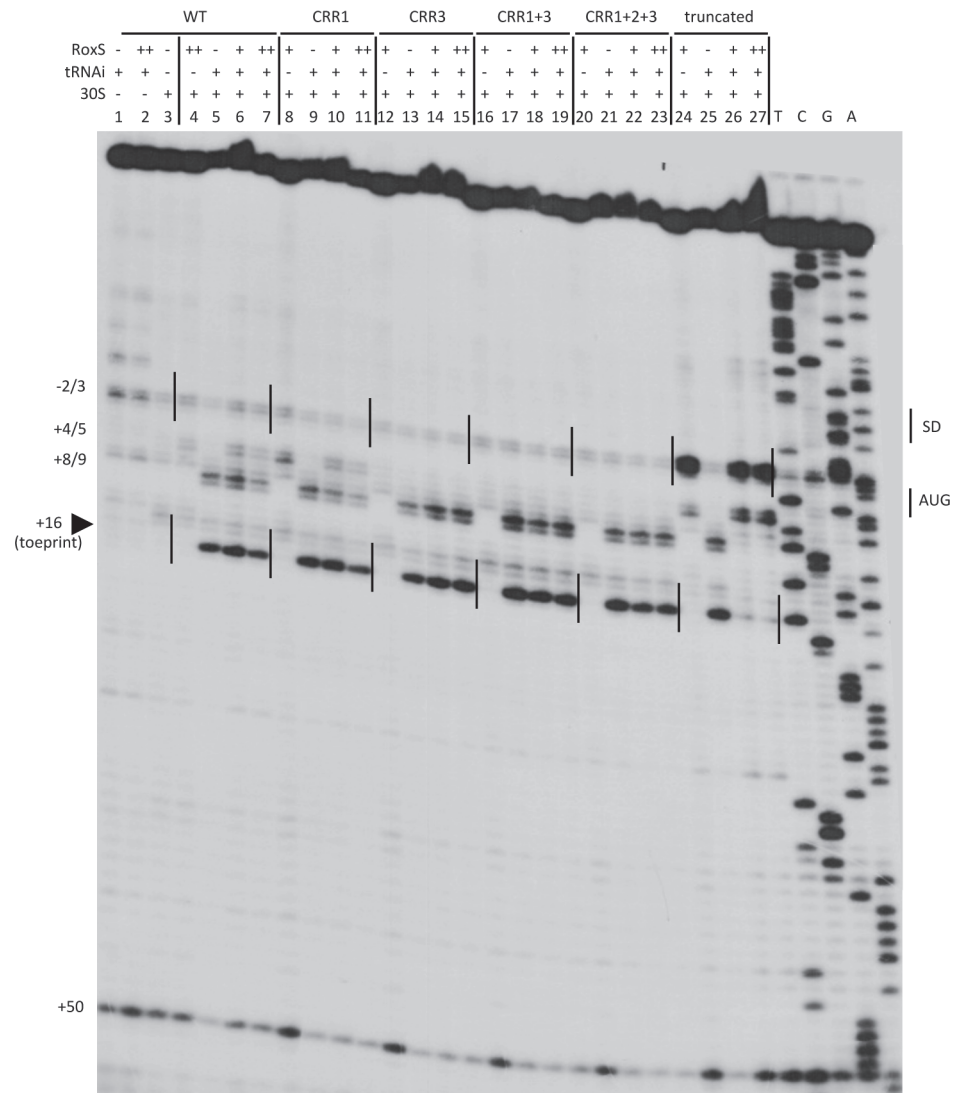


Figure 11. Inhibition of initiation complex formation on the *sucC* mRNA by RoxS *in vitro*. Toeprint analysis of full-length (WT) and various mutant or truncated forms of RoxS bound to the *sucC* mRNA. The major toeprint formed by the 30S ribosomal subunit is indicated at +16 relative to the first nt of the start codon (AUG). A weaker toeprint is also seen around position +8/9, which does not correspond to the functional AUG codon. Both toeprints respond similarly to RoxS binding. Weak binding of full-length RoxS to *sucC* is characterized by RT stops at nts -2/3 and +4/5. Much stronger RT stops are observed with the truncated form of RoxS. The Shine and Dalgarno sequence is indicated by SD. (++) indicates addition of twice the quantity of RoxS (80 nM vs. 40 nM) as in lanes marked with (+).

doi:10.1371/journal.pgen.1004957.g011

more efficient as growth begins to slow down and RoxS expression is essentially completely ResD-dependent in early stationary phase (Fig. 1C). Despite the fact that a number of the surrounding genes show increased expression in the presence of diamide, the thiol stress regulator Spx had little effect on RoxS expression. This is consistent with a recent study by Rochat *et al.* that showed an effect of an *spx* deletion on the neighboring genes but not on *roxS* itself [33]. However, a significant number of genes with functions related to oxidation-reduction reactions or oxidative stress resistance showed increased expression in *B. subtilis* cells lacking RoxS. This surprising result suggests that Δ *roxS* cells are suffering from a deficit of reducing power. The derepression of many members of the Fur regulon, including the *ykuNOP* operon, in the Δ *roxS*

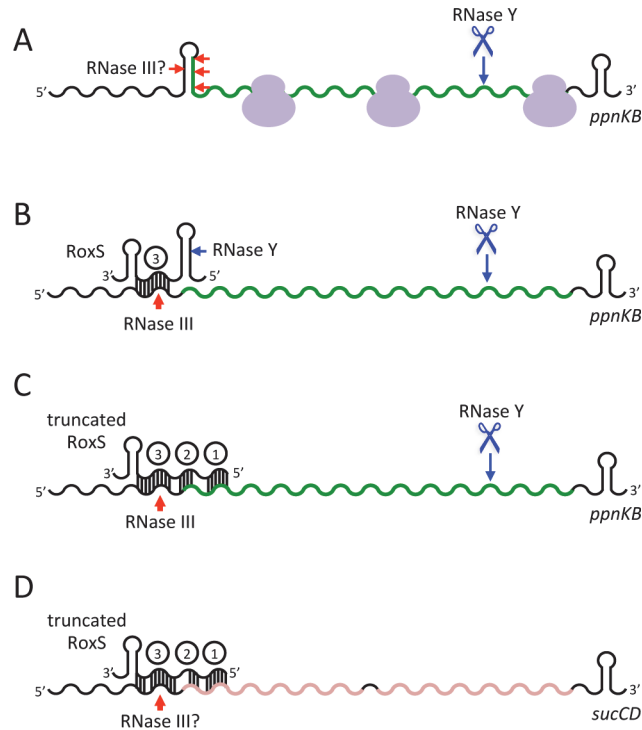


Figure 12. Models of RoxS regulation of the *ppnKB* and *sucCD* mRNAs. (A) RNase Y (blue scissors and arrows) can destabilize the *ppnKB* mRNA in the absence of RoxS by stochastically cleaving between passing ribosomes shown in mauve. *In vitro* data suggests there also a possibility of weak cleavage by RNase III (red arrows) in the secondary structure that can form around the translation initiation site in the absence of RoxS. (B) Binding of RoxS blocks ribosomes from initiating translation of *ppnKB*. RNase III cleaves the duplex formed between CRR3 and *ppnKB* irreversibly inactivating the mRNA for translation. The lack of ribosomes gives RNase Y free access to cleave *ppnKB*. The site of RNase Y cleavage of RoxS is shown (blue arrow). (C) The cleaved form of RoxS forms a more extended hybrid with *ppnKB* that encompasses CRR1-3 and that is as effective at regulating translation and turnover of *ppnKB* as the full-length species. *In vitro* experiments show that the hybrid between the truncated form of RoxS and *ppnKB* is also efficiently cleaved by RNase III. (D) Regulation of the *sucCD* operon requires prior cleavage of RoxS. RNase III is the principal regulator of *sucCD* turnover and we presume the cleavage site is in the RoxS/*sucCD* duplex that encompasses CRR1, 2 and 3.

doi:10.1371/journal.pgen.1004957.g012

deletion strain is consistent with this observation. Since Fur uses reduced iron (Fe^{2+}) as a co-repressor, a deficit in reducing power would be predicted to lead to decreased Fur repressor activity and increased expression of these genes.

We validated the direct role of RoxS in regulation of expression of *ppnKB* at both the level of translation initiation and mRNA turnover (Fig 12). By converting NAD^+ to NADP^+ using ATP or inorganic polyphosphate as a phosphate donor, PpnKB shifts the metabolic balance from the production of energy from respiration, which uses primarily NADH, towards more anabolic reactions that use NADPH as a reducing agent. Expression of RoxS would therefore be expected to limit NADPH production. The increased expression of the *gndA* and *tkt* genes observed in the ΔroxS strain in the transcriptome experiment is consistent with this response. Tkt (transketolase) and GndA (6-phospho-gluconate dehydrogenase) are involved in the pentose phosphate pathway, a major source of NADPH synthesis in the cell. Furthermore, a recent paper has suggested that up to 40% of cellular levels NADPH come from folate metabolism in higher eukaryotes [46]. Interestingly, folate metabolism was a key target of RsaE in *S. aureus* [17,18]. We therefore suggest that one of the physiological roles of RoxS in both *B. subtilis* and *S. aureus* is to turn down expression of genes no longer required under conditions where

electron transport is limited (e.g. NO stress or hypoxia), the intracellular environment is reduced and less NADPH is required. Conversely, the increased expression of *ppnKB*, *gndA* and *tkt* genes observed in the RoxS deletion strain is a consistent response for a cell in need of reducing power.

A direct comparison of the genes affected by the RoxS/RsaE deletion in *B. subtilis* and *S. aureus* showed only four genes in common, namely *sucD*, *pgk*, *citZ* and *yjcG/SA0873* [17,18]. Thus, although the TCA cycle is a common target for this sRNA in both species, the majority of the genes affected are different. This may reflect fundamental differences in the regulation of the expression of RoxS or its targets in relation to their respective ecological niches and circumstances in which they encounter NO. Nevertheless, it provides an interesting example of how a similarly regulated sRNA has evolved to control different targets in two distantly related bacteria.

B. subtilis RoxS acts in concert with ribonucleases to regulate mRNA targets.

The toeprinting analysis showed that RoxS forms a complex with the *ppnKB* mRNA sufficiently stable to prevent ribosome initiation complex formation. Structure probing and reverse transcription stops at nts $-9/10$ of *ppnKB* suggested that the primary *ppnKB*/RoxS interaction occurs *via* CRR3, although we expected more extensive intermolecular pairings. However, it is likely that the 5' stem does not easily unwind in full-length RoxS. In this regard, it is of interest that additional RT stops were seen with the truncated form of RoxS around nts -2 and $+23$, coherent with interactions that extend all the way to the 5' end of the cleaved sRNA. This can be explained by the additional nucleotides in the 5' stem that become available for base-pairing with *ppnKB* upon cleavage of the RoxS sRNA. Intriguingly, this cleavage event is also the first step in RoxS turnover. Although this processed/partially degraded form of RoxS is just as functional as the full-length species in promoting *ppnKB* mRNA turnover *in vivo*, cleavage is not necessary for inhibition of translation initiation complex formation on the *ppnKB* transcript *in vitro*. In contrast, we showed that processing of RoxS is necessary to prevent ribosome binding to the *sucCD* mRNA *in vitro*. Prediction of basepairing interactions suggest that CCR3 binds to the SD sequence in agreement with the toeprinting assays while a second stretch of nts located in the early coding region of *sucC* is complementary to CCR1 of RoxS. We propose that the key to the stabilization of the interaction between RoxS(Y) and *sucCD* is the opening of the 5' stem of RoxS to favor basepairing with the early coding region of *sucC* (Fig. 10A). Although full-length RoxS is unable to bind efficiently to the *sucCD* mRNA *in vitro*, a specific RoxS-dependent degradation of *sucCD* mRNA was observed *in vivo* (Fig. 10) suggesting that a *trans*-acting factor, such as an RNA chaperone, might assist RoxS in the regulatory mechanism. Alternatively, sufficient quantities of the RNase Y cleaved form of RoxS may be generated *in vivo* for regulation of *sucCD*. If it were rapidly co-degraded with its target, this might explain why large quantities of the truncated form do not accumulate *in vivo*. The predicted RNase Y cleavage site in RoxS is in a region of secondary structure, unusual for this endonuclease with a preference for single-stranded RNA [47]. It is therefore possible that RNase Y benefits from its proposed association with the DEAD box helicase CshA [48] to cleave at this site. A number of other sRNAs have been shown to be processed from larger transcripts, e.g. DicF and MicL in *E. coli*, ArcZ in *E. coli* and *Salmonella enterica*, MicX in *Vibrio cholerae* [49–53]. In most of these cases, the processed form is the major form found in the cell and is considered to be the active form of the molecule. In the case of ArcZ, it was shown that while the long form was a better binder of Hfq, only the RNase E-processed species could form a Hfq-dependent complex with its target *rpoS* [54]. In the case studied here, the unprocessed form of RoxS is the major

form found in cells and likely to be the principal regulatory species. Cleavage of the sRNA potentially allows it to diversify and bind to other mRNA targets, essentially creating two functional sRNAs for the price of one.

Hfq has been shown to play an important role in sRNA regulation in the Proteobacteria, but only very few sRNAs have Hfq-dependent regulation in the Firmicutes. We nonetheless addressed the question of whether deletion of the *hfq* gene had an effect on RoxS-dependent down-regulation of the *ppnKB* mRNA, but did not observe any major impact of the *hfq* mutation (S8 Fig.). This result is tempered by the observation that, in the Proteobacteria, over-expression of sRNA has sometimes been shown to by-pass the need for Hfq [54].

Because RoxS binds to the SD sequence and inhibits the initiation complex formation *in vitro*, it clearly points to a role for RoxS in inhibiting *ppnKB* translation. In addition to this regulation, *ppnKB* is controlled at the level of mRNA turnover. First, RNase III can cleave the duplex between *ppnKB* and RoxS (Fig. 12). Cleavage in the SD sequence would immediately and irreversibly render the *ppnKB* mRNA translationally non-functional. A similar mechanism has been previously proposed in the regulation of the *ompA* and *lamB* mRNAs by the MicA sRNA in *Salmonella* [55] and the *sodB* mRNA by RyhB in *E. coli* [56]. *In vitro*, RNase III cleaved the large and irregular helix in the *ppnKB* mRNA in the absence of RoxS binding, albeit weakly. We therefore cannot rule out the involvement of RNase III in the turnover of *ppnKB* in the absence of RoxS *in vivo*; however, this relatively weak structure may not be able to compete efficiently with ribosome initiation *in vivo*. Our *in vivo* data suggest that RNase Y is also an important player in turnover of the *ppnKB* mRNA in both a RoxS-dependent (Fig. 6) and RoxS-independent (Fig. 7) manner. We propose that in the absence of RoxS, RNase Y can cleave the *ppnKB* mRNA occasionally between passing ribosomes (Fig. 12A). Upon inhibition of translation by RoxS, cleavage by RNase Y would be more efficient. Although the role of RNase E in sRNA regulation is now well-established in the Enterobacteria, the equivalent enzyme in Firmicutes, which in most cases do not have RNase E, was not known. Here we show for the first time that RNase Y plays an analogous role in Gram-positive sRNA regulation.

As two endonucleases cannot generally be rate limiting for the initiation of degradation on the same RNA, the fact that the *ppnKB* mRNA half-life increases in both an Δrnc and Δrny mutant suggests that at least two different populations of the *ppnKB* mRNA exist. The simplest interpretation of the data measured under equilibrium conditions in RoxS and RNase deletion strains (Fig. 7) is that RNase III cleaves the population of *ppnKB* bound to RoxS, while RNase Y cleaves the free *ppnKB* population. However, the transient high-level RoxS induction experiment gives a different picture. Indeed, this experiment suggests that RNase Y plays the major role in RoxS-mediated *ppnKB* turnover, while the RoxS-dependent role of RNase III is relatively minor (Fig. 6). The fundamental difference between these two experiments is the amount of RoxS in the cell. We therefore hypothesize that both RNase Y and RNase III can turnover the *ppnKB* mRNA in a RoxS-dependent manner, but that the equilibrium between the two pathways depends on the amount of RoxS in the cell in ways that we do not yet fully understand.

CRR1 and CCR3 are each contained within a 10-nucleotide (nt) sequence duplication CCCCUUGUU that can potentially base pair with the *ppnKB* SD sequence. Surprisingly, mutation of CRR1 had little effect on ribosome binding, while mutation of CRR3 essentially abolished it. Furthermore, the mutation of CRR1 and CRR3 together behaved similarly to the CRR3 mutant alone in both toeprinting assays and in the structure probing assays of the *ppnKB*/RoxS duplex, clearly showing the predominant role of CRR3 in *ppnKB* binding (Fig. 4, 9 and S7 Fig.). The structure of RoxS is most likely an important factor that explains why the two homologous sequences are not functionally redundant for *ppnKB* regulation. However, our data do not rule out a role for CRR1 in the regulation of other targets.

In addition to a whole family of sRNAs in *S. aureus* that contain CRRs [17], at least two other *B. subtilis* sRNAs, CsfG and FsrA [7,57], have CRRs in predicted single stranded regions. FsrA is a member of the Fur regulon. It contains three CRRs, two of which are separated by two nucleotides similar to the CRR2/CRR3 configuration in RoxS. CsfG also has three CRRs and, although it was characterized as an sRNA specific to sporulation in *B. subtilis*, recent evidence has suggested it may also be induced under conditions of oxidative stress [28]. These intriguing overlaps in both structure and regulation are suggestive of a functional redundancy and/or shared mechanisms of action between this class of sRNAs and their targets in Firmicutes.

Materials and Methods

Strains and constructs

Strains and oligonucleotides used are given in S3–S4 Tables, respectively. Strain CCB485 (*roxS::kan*) was constructed using a PCR fragment generated by re-amplifying (oligo pair CC1154/1159) three overlapping PCR fragments corresponding to upstream (oligo pair CC1154/CC1231), downstream (oligo pair CC1233/CC1159) regions of the *roxS* gene and the kanamycin resistance cassette (oligo pair CC1230/CC1232) from plasmid pDG780 [58]. The resulting PCR fragment was used to transform *B. subtilis* W168 (SSB1002) and the correct insertion verified by PCR and sequenced. Strain CCB282 (*roxS::spc*) was constructed by first constructing a plasmid where fragments corresponding to regions upstream (oligo pair RsaE-up-BamHI/RsaE-low-HindIII) and downstream (oligo pair RsaE-up-XhoI/RsaE-low-ApaI) of the *roxS* gene were amplified by PCR, cut with BamHI/HindIII and XhoI/ApaI, respectively and cloned on either side of the spectinomycin resistance cassette in plasmid pBS-Spc [59] cut with the same enzymes. The resulting plasmid was used to transform *B. subtilis* 168 (CCB281) and the correct insertion verified by PCR.

Plasmid pDG-ResDE was made by amplifying the *resDE* gene by PCR using oligo pair CC1222/1223, cutting with SphI and Sall and inserting between the same sites of pDG148 [58].

Plasmid pDG-Ptet-roxS was made from a previously made plasmid (pDG-Ptet-*txpA*/ratA-Plac) containing a XbaI-Pxyl/tet promoter-AatII-*txpA*/ratA-AatII-Plac-BstB1 construct cloned between the BstB1 and XbaI sites of pDG148 [58]. The *roxS* gene was amplified with oligos CC1216/1217 and inserted in the above plasmid cut with AatII and BstB1. The resulting plasmid pDG-Ptet-roxS permits the expression of *roxS* from its native +1 under the control of aTc. The empty vector control pDG-Ptet was made by inserting the hybridized oligos CC1328/1329 between the AatII and BstB1 sites of pDG-Ptet-*txpA*/ratA-Plac (above), creating a HindIII site.

Mutant derivatives of RoxS were created by PCR or overlapping PCR and cloning between the AatII and HindIII sites of pDG-Ptet. The four C's of CRR1 were mutated to four A residues using oligo pair CC1323/1399. The four C's of CRR3 were mutated to four A residues using overlapping oligo pairs CC1160/1327 and CC1326/1399 and reamplified with CC1160/1399. The CRR1 and CRR3 mutants were combined using oligos CC1323/1327 and CC1326/1399 and reamplified with oligos CC1323/1399. RoxS(Y) was made using oligo pair CC1398/1399. The CRR1,2,3 mutant was made by overlapping PCR using oligo pairs CC1323/1324 and CC1325/1399 and reamplified using oligos CC1323/1399. These plasmids were used for PCR amplification of templates for *in vitro* transcription of mutant RoxS RNAs.

RNA isolation and northern blots

RNA was isolated from mid-log phase *B. subtilis* cells growing 2×YT medium either by the glass beads/phenol method described in [60] or by the RNAsnap method described in [61]. Northern blots were performed as described previously [39]. *S. aureus* strains (HG001,

HG001- Δ *srrAB*) were grown to post-exponential phase by inoculating 50 ml of BHI medium with an overnight culture (1:100) at 37°C for 7 h. *S. aureus* total RNA was prepared according to the FastRNA Pro protocol (Qbiogene). After separation on agarose gels (1–2%) containing 20 mM guanidine thiocyanate, RNA was transferred onto Hybond-N+ membranes (Amersham). Detection of transcripts was done with DIG-labeled RNA according to the protocol provided by Roche.

Tiling array and data analysis

Strains CCB281 (wild-type) and CCB282 Δ *roxS* (S3 Table) were used for transcriptome analysis. Cells were grown in 2×YT medium to OD₆₀₀ ~ 0.6. 20 mL aliquots were centrifuged and RNA was prepared by the glass beads method [60], with an additional RQ DNase (Promega) step (0.01 units/μL, 37°C for 30 mins) after the second phenol extraction. RNA concentrations were measured and duplicate samples sent to Roche/Nimblegen for labeling and analysis on second-generation (T2) tiling arrays according to the BaSysBio protocol described in [28]. The data were quantile normalized and moderated t-test p-values were computed for the difference between the Δ *roxS* and WT genetic backgrounds (R package limma [62]). The p-values were converted to q-values to account for multiple testing via control of the False Discovery Rate (FDR) (R package fdrtool [63]). The cut-off value chosen for significant effects was ≥ 2 , with a Q-value of ≤ 0.05 .

Mass spectrometry based quantification: Spectral counting and MS1 label-free approaches

Strains CCB281 (WT) and CCB282 (Δ *roxS*) were used for comparative proteomic analysis. Crude extracts were obtained by trizol (Sigma) extraction, followed by acetone precipitation. Proteins (5 μg) were precipitated with 0.1 M ammonium acetate in 100% methanol, and then resuspended in 50 mM ammonium bicarbonate. After a reduction-alkylation step (5 mM DTT—10 mM iodoacetamide), proteins were digested overnight with 1/25 (W/W) of trypsin and only 3 μg of proteins was vacuum dried. The dried peptides were resuspended in 20 μL of water containing 0.1% formic acid (solvent A). The peptide mixtures were analyzed using a NanoLC-2DPlus system (with nanoFlex ChiP module; Eksigent, ABSciex, Concord, Ontario, Canada) coupled to a TripleTOF 5600 mass spectrometer (ABSciex) operating in positive mode. Each sample (5 μl; 750 ng) was loaded on a ChIP C-18 precolumn (300 μm ID × 5 mm ChromXP; Eksigent) at 2 μL/min in solvent A. After 10 min of desalting and concentration in the trap, the pre-column was switched online with the analytical ChIP C-18 analytical column (75 μm ID × 15 cm ChromXP; Eksigent) equilibrated in 95% solvent A and 5% solvent B (0.1% formic acid in acetonitrile). Peptides were eluted by using a 5%–40% gradient of solvent B for 120 min at a flow rate of 300 nL/min. The TripleTOF 5600 was operated in data-dependent acquisition mode (DDA) with Analyst software (v1.6, ABSciex). Survey MS scans were acquired during 250 ms in the 350–1250 m/z range. Up to 20 of the most intense multiply charged ions (2+ to 4+) were selected for Collision-Induced Dissociation (CID) fragmentation, if they exceeded a 150 counts per second intensity threshold. Ions were fragmented using a rolling collision energy script within a 60 ms accumulation time and an exclusion time of 15s. This so-called “Top20” method, with a constant cycle time of 1.5s, was set to high-sensitivity mode.

Data were searched against the *B. subtilis* strain 168 database from SwissProt (release 2013-11-20). The first algorithm used was Mascot (version 2.2, Matrix Science, London, UK) through the ProteinScape 3.1 package (Bruker). Variable peptide modifications allowed during the search were: N-acetyl (protein), carbamidomethylation (C) and oxidation (M). Mass tolerances in MS and MS/MS were set to 20 ppm and 0.5 Da, respectively. Two missed trypsin

cleavages sites were allowed. Peptide identifications obtained from Mascot were validated with a peptide false discovery rate (FDR) of 1%. A Spectral Counting quantitative strategy was first carried on using the Mascot identification results and Proteinscape 3.1 package [64,65]. To normalize the data, a correction factor was applied for each condition according to the average total spectra number for all samples.

The Paragon algorithm (ProteinPilot package, AB Sciex) was then used to perform a second database search on the same nanoLC-MS/MS dataset and with the same decoy *B. subtilis* database. Proteins validated by Paragon at FDR 1% were submitted to a MS1 label-free quantification. For that purpose, only non-modified and unshared peptides were considered, as well as the Paragon identification confidence threshold set at 99%. Precursor ions fulfilling these criteria were transferred into PeakView package (v 2.0 with Protein Quantitation plug-in, AB Sciex) and their corresponding eXtracted Ion Chromatograms (XIC) were automatically integrated, using the following parameters: RT window ± 2 min, MS tolerance ± 0.05 Da. To normalize and further process the MS1 label-free data, MarkerView software (v 1.2, ABSciex) was used: a correction factor was first applied for each condition according to the total area sum function. The statistical module from MarkerView finally allowed us to perform a Principle Component Analysis (PCA) and a Student t-test on the repeated triplicate experiments.

Primer extension assays

Primer extension assays were performed as described previously on total RNA [59].

Toeprinting assays

The RNA fragments were transcribed *in vitro* from PCR fragments containing the leader regions and coding sequences of *ppnKB* (oligos ppnKB T7 fw/ppnKB rev2), *ykuN* (oligos ykuN T7 fw/ykuN rev 2) and *sucC* (oligos sucC T7 fw/sucC rev2). RoxS and its mutant derivatives were made similarly using PCR fragments (oligos RsaE T7 fw/RsaE rev) amplified from their respective plasmids. The transcribed RNAs were purified by 8% polyacrylamide-8 M urea gel electrophoresis. After elution in 0.5 M ammonium acetate/1 mM EDTA buffer, the RNAs were precipitated twice with ethanol. The 5' end-labeling of dephosphorylated DNA oligonucleotides was performed with T4 polynucleotide kinase and [γ - 32 P]ATP. Before use, RNAs were re-natured by incubation at 90°C for 2 min in the absence of magnesium and salt, 1 min on ice, followed by an incubation step at 37°C for 15 mins in TMN buffer (20 mM Tris-acetate pH 7.5, 10 mM magnesium-acetate, 150 mM Na-acetate).

Toeprints were performed with *E. coli* 30S subunits. The preparation ribosomal subunits, the formation of a simplified translational initiation complex with mRNA, and the extension inhibition conditions were described according to Fechter *et al.* [66]. Standard conditions contained 15 nM RNA transcript annealed to a 5' end-labeled oligonucleotide (ppnKB rev1, ykuN rev1: complementary to codons 16 to 22; and sucC rev1: complementary to codons 24 to 31) 250 nM *E. coli* 30S ribosomal subunits (250 nM), and 40 to 80 nM of RoxS in 10 μ l of buffer containing 20 mM Tris-acetate, pH 7.5, 60 mM NH₄Cl, 10 mM magnesium acetate, and 3 mM β -mercaptoethanol. After 10 mins at 37°C, the initiator tRNA (1 μ M) was added and the reaction was incubated for a further 5 mins at 37°C. Reverse transcription was conducted with one unit of AMV reverse transcriptase for 15 mins at 37°C.

Structure probing experiments

RoxS-*ppnKB* mRNA formation was carried out at 37°C for 15 mins in TMN buffer containing 50 mM Hepes-NaOH pH 7.5, MgCl₂ 5 mM, KCl 50 mM. The concentrations of RoxS or its derivatives were 40 nM and 80 nM. Enzymatic hydrolysis was performed with unlabeled *ppnKB*

(0.5 pmol) in 10 μ l of TMN, in the presence of 1 μ g carrier tRNA at 37°C for 5 mins: RNase T1 (0.002 units, Thermo scientific), RNase V1 (1 unit, Ambion), purified *B. subtilis* RNase III (165 nM, 330 nM, 660 nM). The reactions were stopped by phenol extraction followed by RNA precipitation. The enzymatic cleavages were detected by primer extension with reverse transcriptase according to [67].

Supporting Information

S1 Fig. Chromosomal context around the *rsaE/roxS* gene in *S. aureus* and *B. subtilis*. Conserved genes are in similar colors. Promoters are indicated by black arrows, transcription terminators are shown by lollipops. Gene functions and pertinent expression patterns from Nicolas *et al.* [28] are indicated below the figure.

(TIF)

S2 Fig. Alignment of RsaE/RoxS sequences from different *Staphylococci* and *Bacilli*. The RoxS sequences are boxed in blue. Likely -35 and extended -10 sequences are boxed in mauve and the putative ResD binding site is boxed in green. Positions showing 100% conservation are indicated by asterisks. Abbreviations are as follows: Sepi, *S. epidermis*; SauCol, *S. aureus* Colindale strain; Shae, *S. haemophilus*; Ban, *B. anthracis*; SauNew, *S. aureus* Newman strain; Bli, *B. lichiniiformis*; Bpu, *B. pumilus*; Bsub, *B. subtilis*.

(TIF)

S3 Fig. Effect of RoxS on *ykuN* expression. (A) Northern blot showing effect of RoxS deletion on *ykuN* expression. The blot was re-probed for 16S rRNA using oligo CC058. (B) Comparison of efficiency of RoxS toeprint inhibition on *ppnKB* and *ykuN* mRNAs. RoxS concentrations were 40, 80 nM for *ppnKB* and 40, 80, 150 nM for *ykuN*. The 30S toeprint +16 is labeled, as is the RT pause at -9/10 for *ppnKB*.

(TIF)

S4 Fig. Functional annotation chart of potential RoxS targets produced by CopraRNA. The input RoxS sequences were from *B. subtilis*, *B. lichiniiformis*, *B. cereus*, *B. pumilus* and *B. thuringiensis*. The enrichment score cut-off was ≥ 1.0 . The X-axis represents the different functional categories, while the Y-axis shows all predicted RoxS targets with a P-value of ≤ 0.01 . Functional categories belonging to the same overall group have similar colors, with darker colors representing smaller P-values.

(TIF)

S5 Fig. 5'-mapping of RoxS degradation intermediate observed in strains lacking RNase J1 by primer extension. The 5' ends corresponding to the transcriptional start site (+1) and degradation intermediate (D) are shown. Primer extension was performed with oligo CC1363. The sequence is labeled as its complement for direct read-out. Strains used were SSB1002 (WT), CCB434 Δ *rnjA* (J1) and CCB441 Δ *rnjY* (Y).

(TIF)

S6 Fig. The truncated form of RoxS is functional *in vivo*. (A) Northern blot of total RNA isolated from strain CCB498 (Δ *roxS* + pDG-Ptet-*roxS*) and CCB582 (Δ *roxS* + pDG-Ptet-*roxS*(Y)) at times after the addition of 40 μ g/mL aTc. The (agarose gel) blot was probed for *ppnKB* (oligo CC964), then re-probed for *sucCD* (oligo CC1408) and 16S rRNA (oligo CC058). The RNAs were also run on a polyacrylamide gel and probed for RoxS. (B) Quantification of Northern blots shown in panel A. *ppnKB* and *sucCD* mRNAs were normalized to 16S rRNA and to the T0 sample (right hand Y-axis). RoxS was normalized to 16S rRNA only (left hand Y-axis).

(TIF)

S7 Fig. Structure probing of *ppnKB* bound to wild type (WT) and various mutant/cleaved forms of RoxS. (A) Structure probing by RNase T1. The *ppnKB* mRNA was hybridized to 40 nM and 80 nM RoxS, digested by RNase T1 and assayed by primer extension using oligo *ppnKB* rev1. Key changes are labeled, as is the strong RT stop at -9/10 (arrow) provoked by RoxS binding to *ppnKB* mRNA (B) Structure probing by RNase V1. Legend as for panel A. Sites of RNase T1 and V1 cleavage are shown in [Fig. 8A and B](#).

(TIF)

S8 Fig. Hfq is not necessary for RoxS-dependent inhibition of *ppnKB* expression *in vivo*.

(A) Northern of total RNA isolated from strain CCB505 (Δ *roxS* + empty vector) and CCB498 (Δ *roxS* + pDG-Ptet-roxS) at times after the addition of 40 μ g/mL aTc. The blot was re-probed for 16S rRNA (oligo CC058; [S4 Table](#)) as a loading control. (B) Same as panel A using Hfq mutant strains CCB660 (Δ *roxS* Δ *hfq* + empty vector) and CCB661 (Δ *roxS* Δ *hfq* + pDG-Ptet-roxS). (C) Quantification of Northern blots shown in panels A and B. *ppnKB* mRNA was normalized to 16S rRNA and to the T0 sample (right hand Y-axis). RoxS was normalized to 16S rRNA only (left hand Y-axis).

(TIF)

S1 Table. Comparison of expression of Δ *roxS* and wild-type strains by proteome analysis (LC-MS/MS). The experiment was performed in triplicate. The number of replicates in which peptides were detected is given. For spectral counting only peptides with an average ≥ 5 spectra were retained. For MS1 filtering, only those with a P-value ≤ 0.05 were retained. Only proteins showing a Δ *roxS*/WT ratio ≥ 1.5 fold difference by both methods are included in the final table. The regulon to which the candidates belong is indicated. Potential direct targets are indicated with their rank and prediction program: (C) CopraRNA, (T) TargetRNA, (P) RNApredator. Bold-face type (in gene symbol lane) indicates candidates also found by transcriptome analysis.

(XLSX)

S2 Table. Comparison of expression of Δ *roxS* and wild-type strains by tiling array. The experiment was performed in duplicate. Only mRNAs showing a Δ *roxS*/WT ratio ≥ 2.0 fold and a q-value ≤ 0.05 are included in the final table. The regulon to which the candidates belong is indicated. Potential direct targets are indicated with their rank and prediction program: (C) CopraRNA, (T) TargetRNA, (P) RNApredator. Bold-face type indicates candidates also found by proteome analysis. Column H: proteome data showing Δ *roxS*/WT ratio for Spectral Counting (SC)/ Δ *roxS*/WT ratio for MS1 Filtering (MS1)/ average number of peptides in mutant/p-value for MS1 filtering. nd: not determined.

(XLSX)

S3 Table. Strains used in this study.

(DOC)

S4 Table. Oligonucleotides used in this study. Restriction sites are in lower case letters.

T7 promoter sequences are underlined.

(DOC)

Acknowledgments

We thank M. Nakano, John Helmann and T. Msadek for the kind gift of the *B. subtilis* Δ *resDE* and Δ *hfq* strains, and the *S. aureus* HG001- Δ *srrAB* strain, respectively. We are grateful to P. Hammann and J. Chicher for proteomics analysis and P. Bouloc for the tip on the transient

expression of the Ptet promoter. We thank M. Springer, E. Hajnsdorf, M. Guillier, F. Fontaine, M. Nakano, F. Rappaport, A. Lescure, E. Westhof, and T. Geissmann for helpful discussions.

Author Contributions

Conceived and designed the experiments: SD FB EL PR CC. Performed the experiments: SD FB EL CR ACH NQ. Analyzed the data: SD FB EL LK PN PR CC. Wrote the paper: SD FB EL PR CC.

References

1. Storz G, Vogel J, Wassarman KM (2011) Regulation by small RNAs in bacteria: expanding frontiers. *Mol Cell* 43: 880–891. doi: [10.1016/j.molcel.2011.08.022](https://doi.org/10.1016/j.molcel.2011.08.022) PMID: [21925377](https://pubmed.ncbi.nlm.nih.gov/21925377/)
2. Caldelari I, Chao Y, Romby P, Vogel J (2013) RNA-mediated regulation in pathogenic bacteria. *Cold Spring Harb Perspect Med* 3: a010298. doi: [10.1101/cshperspect.a010298](https://doi.org/10.1101/cshperspect.a010298) PMID: [24003243](https://pubmed.ncbi.nlm.nih.gov/24003243/)
3. Ramirez-Pena E, Trevino J, Liu Z, Perez N, Sumbly P (2010) The group A *Streptococcus* small regulatory RNA FasX enhances streptokinase activity by increasing the stability of the *ska* mRNA transcript. *Mol Microbiol* 78: 1332–1347. doi: [10.1111/j.1365-2958.2010.07427.x](https://doi.org/10.1111/j.1365-2958.2010.07427.x) PMID: [21143309](https://pubmed.ncbi.nlm.nih.gov/21143309/)
4. Obana N, Shirahama Y, Abe K, Nakamura K (2010) Stabilization of *Clostridium perfringens* collagenase mRNA by VR-RNA-dependent cleavage in 5' leader sequence. *Mol Microbiol* 77: 1416–1428. doi: [10.1111/j.1365-2958.2010.07258.x](https://doi.org/10.1111/j.1365-2958.2010.07258.x) PMID: [20572941](https://pubmed.ncbi.nlm.nih.gov/20572941/)
5. Opdyke JA, Fozo EM, Hemm MR, Storz G (2011) RNase III participates in GadY-dependent cleavage of the *gadX-gadW* mRNA. *J Mol Biol* 406: 29–43. doi: [10.1016/j.jmb.2010.12.009](https://doi.org/10.1016/j.jmb.2010.12.009) PMID: [21147125](https://pubmed.ncbi.nlm.nih.gov/21147125/)
6. Pfeiffer V, Papenfort K, Lucchini S, Hinton JC, Vogel J (2009) Coding sequence targeting by MicC RNA reveals bacterial mRNA silencing downstream of translational initiation. *Nat Struct Mol Biol* 16: 840–846. doi: [10.1038/nsmb.1631](https://doi.org/10.1038/nsmb.1631) PMID: [19620966](https://pubmed.ncbi.nlm.nih.gov/19620966/)
7. Gaballa A, Antelmann H, Aguilar C, Khakh SK, Song KB, et al. (2008) The *Bacillus subtilis* iron-sparing response is mediated by a Fur-regulated small RNA and three small, basic proteins. *Proc Natl Acad Sci U S A* 105: 11927–11932. doi: [10.1073/pnas.0711752105](https://doi.org/10.1073/pnas.0711752105) PMID: [18697947](https://pubmed.ncbi.nlm.nih.gov/18697947/)
8. Heidrich N, Chinali A, Gerth U, Brantl S (2006) The small untranslated RNA SR1 from the *Bacillus subtilis* genome is involved in the regulation of arginine catabolism. *Mol Microbiol* 62: 520–536. PMID: [17020585](https://pubmed.ncbi.nlm.nih.gov/17020585/)
9. Gimpel M, Preis H, Barth E, Gramzow L, Brantl S (2012) SR1 - a small RNA with two remarkably conserved functions. *Nucleic Acids Res* 40: 11659–11672. doi: [10.1093/nar/gks895](https://doi.org/10.1093/nar/gks895) PMID: [23034808](https://pubmed.ncbi.nlm.nih.gov/23034808/)
10. Smaldone GT, Antelmann H, Gaballa A, Helmann JD (2012) The FsrA sRNA and FbpB protein mediate the iron-dependent induction of the *Bacillus subtilis* *lutABC* iron-sulfur-containing oxidases. *J Bacteriol* 194: 2586–2593. doi: [10.1128/JB.05567-11](https://doi.org/10.1128/JB.05567-11) PMID: [22427629](https://pubmed.ncbi.nlm.nih.gov/22427629/)
11. Smaldone GT, Revelles O, Gaballa A, Sauer U, Antelmann H, et al. (2012) A global investigation of the *Bacillus subtilis* iron-sparing response identifies major changes in metabolism. *J Bacteriol* 194: 2594–2605. doi: [10.1128/JB.05990-11](https://doi.org/10.1128/JB.05990-11) PMID: [22389480](https://pubmed.ncbi.nlm.nih.gov/22389480/)
12. Huntzinger E, Boisset S, Saveanu C, Benito Y, Geissmann T, et al. (2005) *Staphylococcus aureus* RNAlII and the endoribonuclease III coordinately regulate *spa* gene expression. *EMBO J* 24: 824–835. doi: [10.1038/sj.emboj.7600572](https://doi.org/10.1038/sj.emboj.7600572) PMID: [15678100](https://pubmed.ncbi.nlm.nih.gov/15678100/)
13. Hammerle H, Amman F, Vecerek B, Stulke J, Hofacker I, et al. (2014) Impact of Hfq on the *Bacillus subtilis* transcriptome. *PLoS One* 9: e98661. doi: [10.1371/journal.pone.0098661](https://doi.org/10.1371/journal.pone.0098661) PMID: [24932523](https://pubmed.ncbi.nlm.nih.gov/24932523/)
14. Dambach M, Irnov I, Winkler WC (2013) Association of RNAs with *Bacillus subtilis* Hfq. *PLoS One* 8: e55156. doi: [10.1371/journal.pone.0055156](https://doi.org/10.1371/journal.pone.0055156) PMID: [23457461](https://pubmed.ncbi.nlm.nih.gov/23457461/)
15. Even S, Pellegrini O, Zig L, Labas V, Vinh J, et al. (2005) Ribonucleases J1 and J2: two novel endoribonucleases in *B. subtilis* with functional homology to *E. coli* RNase E. *Nucleic Acids Res* 33: 2141–2152. doi: [10.1093/nar/gki505](https://doi.org/10.1093/nar/gki505) PMID: [15831787](https://pubmed.ncbi.nlm.nih.gov/15831787/)
16. Mathy N, Benard L, Pellegrini O, Daou R, Wen T, et al. (2007) 5'-to-3' exoribonuclease activity in bacteria: role of RNase J1 in rRNA maturation and 5' stability of mRNA. *Cell* 129: 681–692. PMID: [17512403](https://pubmed.ncbi.nlm.nih.gov/17512403/)
17. Geissmann T, Chevalier C, Cros MJ, Boisset S, Fechter P, et al. (2009) A search for small noncoding RNAs in *Staphylococcus aureus* reveals a conserved sequence motif for regulation. *Nucleic Acids Res* 37: 7239–7257. doi: [10.1093/nar/gkp668](https://doi.org/10.1093/nar/gkp668) PMID: [19786493](https://pubmed.ncbi.nlm.nih.gov/19786493/)
18. Bohn C, Rigoulay C, Chabelskaya S, Sharma CM, Marchais A, et al. (2010) Experimental discovery of small RNAs in *Staphylococcus aureus* reveals a riboregulator of central metabolism. *Nucleic Acids Res* 38: 6620–6636. doi: [10.1093/nar/gkq462](https://doi.org/10.1093/nar/gkq462) PMID: [20511587](https://pubmed.ncbi.nlm.nih.gov/20511587/)

19. Song J, Lays C, Vandenesch F, Benito Y, Bes M, et al. (2012) The expression of small regulatory RNAs in clinical samples reflects the different life styles of *Staphylococcus aureus* in colonization vs. infection. PLoS One 7: e37294. doi: [10.1371/journal.pone.0037294](https://doi.org/10.1371/journal.pone.0037294) PMID: [22629378](https://pubmed.ncbi.nlm.nih.gov/22629378/)
20. Demple B (1999) Genetic responses against nitric oxide toxicity. Braz J Med Biol Res 32: 1417–1427. PMID: [10559844](https://pubmed.ncbi.nlm.nih.gov/10559844/)
21. Crane BR, Sudhamsu J, Patel BA (2010) Bacterial nitric oxide synthases. Annu Rev Biochem 79: 445–470. doi: [10.1146/annurev-biochem-062608-103436](https://doi.org/10.1146/annurev-biochem-062608-103436) PMID: [20370423](https://pubmed.ncbi.nlm.nih.gov/20370423/)
22. Gusarov I, Nudler E (2005) NO-mediated cytoprotection: instant adaptation to oxidative stress in bacteria. Proc Natl Acad Sci U S A 102: 13855–13860. doi: [10.1073/pnas.0504307102](https://doi.org/10.1073/pnas.0504307102) PMID: [16172391](https://pubmed.ncbi.nlm.nih.gov/16172391/)
23. Shatalin K, Gusarov I, Avetissova E, Shatalina Y, McQuade LE, et al. (2008) *Bacillus anthracis*-derived nitric oxide is essential for pathogen virulence and survival in macrophages. Proc Natl Acad Sci U S A 105: 1009–1013. doi: [10.1073/pnas.0710950105](https://doi.org/10.1073/pnas.0710950105) PMID: [18215992](https://pubmed.ncbi.nlm.nih.gov/18215992/)
24. Hochgrafe F, Wolf C, Fuchs S, Liebeke M, Lalk M, et al. (2008) Nitric oxide stress induces different responses but mediates comparable protein thiol protection in *Bacillus subtilis* and *Staphylococcus aureus*. J Bacteriol 190: 4997–5008. doi: [10.1128/JB.01846-07](https://doi.org/10.1128/JB.01846-07) PMID: [18487332](https://pubmed.ncbi.nlm.nih.gov/18487332/)
25. Gusarov I, Shatalin K, Starodubtseva M, Nudler E (2009) Endogenous nitric oxide protects bacteria against a wide spectrum of antibiotics. Science 325: 1380–1384. doi: [10.1126/science.1175439](https://doi.org/10.1126/science.1175439) PMID: [19745150](https://pubmed.ncbi.nlm.nih.gov/19745150/)
26. van Sorge NM, Beasley FC, Gusarov I, Gonzalez DJ, von Kockritz-Blickwede M, et al. (2013) Methicillin-resistant *Staphylococcus aureus* bacterial nitric-oxide synthase affects antibiotic sensitivity and skin abscess development. J Biol Chem 288: 6417–6426. doi: [10.1074/jbc.M112.448738](https://doi.org/10.1074/jbc.M112.448738) PMID: [23322784](https://pubmed.ncbi.nlm.nih.gov/23322784/)
27. Gusarov I, Gautier L, Smolentseva O, Shamovsky I, Eremina S, et al. (2013) Bacterial nitric oxide extends the lifespan of *C. elegans*. Cell 152: 818–830. doi: [10.1016/j.cell.2012.12.043](https://doi.org/10.1016/j.cell.2012.12.043) PMID: [23415229](https://pubmed.ncbi.nlm.nih.gov/23415229/)
28. Nicolas P, Mader U, Dervyn E, Rochat T, Leduc A, et al. (2012) Condition-dependent transcriptome reveals high-level regulatory architecture in *Bacillus subtilis*. Science 335: 1103–1106. doi: [10.1126/science.1206848](https://doi.org/10.1126/science.1206848) PMID: [22383849](https://pubmed.ncbi.nlm.nih.gov/22383849/)
29. Baruah A, Lindsey B, Zhu Y, Nakano MM (2004) Mutational analysis of the signal-sensing domain of ResE histidine kinase from *Bacillus subtilis*. J Bacteriol 186: 1694–1704. doi: [10.1128/JB.186.6.1694-1704.2004](https://doi.org/10.1128/JB.186.6.1694-1704.2004) PMID: [14996800](https://pubmed.ncbi.nlm.nih.gov/14996800/)
30. Kinkel TL, Roux CM, Dunman PM, Fang FC (2013) The *Staphylococcus aureus* SrrAB two-component system promotes resistance to nitrosative stress and hypoxia. MBio 4: e00696–00613. doi: [10.1128/mBio.00696-13](https://doi.org/10.1128/mBio.00696-13) PMID: [24222487](https://pubmed.ncbi.nlm.nih.gov/24222487/)
31. Hartig E, Geng H, Hartmann A, Hubacek A, Munch R, et al. (2004) *Bacillus subtilis* ResD induces expression of the potential regulatory genes *yclJK* upon oxygen limitation. J Bacteriol 186: 6477–6484. doi: [10.1128/JB.186.19.6477-6484.2004](https://doi.org/10.1128/JB.186.19.6477-6484.2004) PMID: [15375128](https://pubmed.ncbi.nlm.nih.gov/15375128/)
32. Henares B, Kommineni S, Chumsakul O, Ogasawara N, Ishikawa S, et al. (2014) The ResD Response Regulator, through Functional Interaction with NsrR and Fur, Plays Three Distinct Roles in *Bacillus subtilis* Transcriptional Control. J Bacteriol 196: 493–503. doi: [10.1128/JB.01166-13](https://doi.org/10.1128/JB.01166-13) PMID: [24214949](https://pubmed.ncbi.nlm.nih.gov/24214949/)
33. Rochat T, Nicolas P, Delumeau O, Rabatinova A, Korelusova J, et al. (2012) Genome-wide identification of genes directly regulated by the pleiotropic transcription factor Spx in *Bacillus subtilis*. Nucleic Acids Res 40: 9571–9583. doi: [10.1093/nar/gks755](https://doi.org/10.1093/nar/gks755) PMID: [22904090](https://pubmed.ncbi.nlm.nih.gov/22904090/)
34. Nakano MM (2002) Induction of ResDE-dependent gene expression in *Bacillus subtilis* in response to nitric oxide and nitrosative stress. J Bacteriol 184: 1783–1787. doi: [10.1128/JB.184.6.1783-1787.2002](https://doi.org/10.1128/JB.184.6.1783-1787.2002) PMID: [11872732](https://pubmed.ncbi.nlm.nih.gov/11872732/)
35. Antelmann H, Engelmann S, Schmid R, Sorokin A, Lapidus A, et al. (1997) Expression of a stress- and starvation-induced *dps/pexB*-homologous gene is controlled by the alternative sigma factor sigmaB in *Bacillus subtilis*. J Bacteriol 179: 7251–7256. PMID: [9393687](https://pubmed.ncbi.nlm.nih.gov/9393687/)
36. You C, Sekowska A, Francetic O, Martin-Verstraete I, Wang Y, et al. (2008) Spx mediates oxidative stress regulation of the methionine sulfoxide reductases operon in *Bacillus subtilis*. BMC Microbiol 8: 128. doi: [10.1186/1471-2180-8-128](https://doi.org/10.1186/1471-2180-8-128) PMID: [18662407](https://pubmed.ncbi.nlm.nih.gov/18662407/)
37. Kiran MD, Bala S, Hirshberg M, Balaban N (2010) YhgC protects *Bacillus anthracis* from oxidative stress. Int J Artif Organs.
38. Wang ZQ, Lawson RJ, Buddha MR, Wei CC, Crane BR, et al. (2007) Bacterial flavodoxins support nitric oxide production by *Bacillus subtilis* nitric-oxide synthase. J Biol Chem 282: 2196–2202. PMID: [17127770](https://pubmed.ncbi.nlm.nih.gov/17127770/)
39. Durand S, Gilet L, Bessieres P, Nicolas P, Condon C (2012) Three essential ribonucleases-RNase Y, J1, and III-control the abundance of a majority of *Bacillus subtilis* mRNAs. PLoS Genet 8: e1002520. doi: [10.1371/journal.pgen.1002520](https://doi.org/10.1371/journal.pgen.1002520) PMID: [22412379](https://pubmed.ncbi.nlm.nih.gov/22412379/)

40. Tjaden B (2012) Computational identification of sRNA targets. *Methods Mol Biol* 905: 227–234. doi: [10.1007/978-1-61779-949-5_14](https://doi.org/10.1007/978-1-61779-949-5_14) PMID: [22736007](https://pubmed.ncbi.nlm.nih.gov/22736007/)
41. Wright PR, Richter AS, Papenfort K, Mann M, Vogel J, et al. (2013) Comparative genomics boosts target prediction for bacterial small RNAs. *Proc Natl Acad Sci U S A* 110: E3487–3496. doi: [10.1073/pnas.1303248110](https://doi.org/10.1073/pnas.1303248110) PMID: [23980183](https://pubmed.ncbi.nlm.nih.gov/23980183/)
42. Eggenhofer F, Tafer H, Stadler PF, Hofacker IL (2011) RNAPredator: fast accessibility-based prediction of sRNA targets. *Nucleic Acids Res* 39: W149–154. doi: [10.1093/nar/gkr467](https://doi.org/10.1093/nar/gkr467) PMID: [21672960](https://pubmed.ncbi.nlm.nih.gov/21672960/)
43. Geng H, Nakano S, Nakano MM (2004) Transcriptional activation by *Bacillus subtilis* ResD: tandem binding to target elements and phosphorylation-dependent and -independent transcriptional activation. *J Bacteriol* 186: 2028–2037. doi: [10.1128/JB.186.7.2028-2037.2004](https://doi.org/10.1128/JB.186.7.2028-2037.2004) PMID: [15028686](https://pubmed.ncbi.nlm.nih.gov/15028686/)
44. Georgellis D, Kwon O, Lin EC (2001) Quinones as the redox signal for the arc two-component system of bacteria. *Science* 292: 2314–2316. PMID: [11423658](https://pubmed.ncbi.nlm.nih.gov/11423658/)
45. Ye RW, Tao W, Bedzyk L, Young T, Chen M, et al. (2000) Global gene expression profiles of *Bacillus subtilis* grown under anaerobic conditions. *J Bacteriol* 182: 4458–4465. PMID: [10913079](https://pubmed.ncbi.nlm.nih.gov/10913079/)
46. Fan J, Ye J, Kamphorst JJ, Shlomi T, Thompson CB, et al. (2014) Quantitative flux analysis reveals folate-dependent NADPH production. *Nature* 510: 298–302. doi: [10.1038/nature13236](https://doi.org/10.1038/nature13236) PMID: [24805240](https://pubmed.ncbi.nlm.nih.gov/24805240/)
47. Shahbadian K, Jamalli A, Zig L, Putzer H (2009) RNase Y, a novel endoribonuclease, initiates riboswitch turnover in *Bacillus subtilis*. *EMBO J* 28: 3523–3533. doi: [10.1038/emboj.2009.283](https://doi.org/10.1038/emboj.2009.283) PMID: [19779461](https://pubmed.ncbi.nlm.nih.gov/19779461/)
48. Lehnik-Habrink M, Rempeters L, Kovacs AT, Wrede C, Baierlein C, et al. (2013) DEAD-Box RNA helicases in *Bacillus subtilis* have multiple functions and act independently from each other. *J Bacteriol* 195: 534–544. doi: [10.1128/JB.01475-12](https://doi.org/10.1128/JB.01475-12) PMID: [23175651](https://pubmed.ncbi.nlm.nih.gov/23175651/)
49. Faubladiere M, Cam K, Bouche JP (1990) *Escherichia coli* cell division inhibitor DicF-RNA of the dicB operon. Evidence for its generation in vivo by transcription termination and by RNase III and RNase E-dependent processing. *J Mol Biol* 212: 461–471. PMID: [1691299](https://pubmed.ncbi.nlm.nih.gov/1691299/)
50. Guo MS, Updegrove TB, Gogol EB, Shabalina SA, Gross CA, et al. (2014) MicL, a new sigmaE-dependent sRNA, combats envelope stress by repressing synthesis of Lpp, the major outer membrane lipoprotein. *Genes Dev* 28: 1620–1634. doi: [10.1101/gad.243485.114](https://doi.org/10.1101/gad.243485.114) PMID: [25030700](https://pubmed.ncbi.nlm.nih.gov/25030700/)
51. Papenfort K, Said N, Welsink T, Lucchini S, Hinton JC, et al. (2009) Specific and pleiotropic patterns of mRNA regulation by ArcZ, a conserved, Hfq-dependent small RNA. *Mol Microbiol* 74: 139–158. doi: [10.1111/j.1365-2958.2009.06857.x](https://doi.org/10.1111/j.1365-2958.2009.06857.x) PMID: [19732340](https://pubmed.ncbi.nlm.nih.gov/19732340/)
52. Mandin P, Gottesman S (2010) Integrating anaerobic/aerobic sensing and the general stress response through the ArcZ small RNA. *EMBO J* 29: 3094–3107. doi: [10.1038/emboj.2010.179](https://doi.org/10.1038/emboj.2010.179) PMID: [20683441](https://pubmed.ncbi.nlm.nih.gov/20683441/)
53. Davis BM, Waldor MK (2007) RNase E-dependent processing stabilizes MicX, a *Vibrio cholerae* sRNA. *Mol Microbiol* 65: 373–385. doi: [10.1111/j.1365-2958.2007.05796.x](https://doi.org/10.1111/j.1365-2958.2007.05796.x) PMID: [17590231](https://pubmed.ncbi.nlm.nih.gov/17590231/)
54. Soper T, Mandin P, Majdalani N, Gottesman S, Woodson SA (2010) Positive regulation by small RNAs and the role of Hfq. *Proc Natl Acad Sci U S A* 107: 9602–9607. doi: [10.1073/pnas.1004435107](https://doi.org/10.1073/pnas.1004435107) PMID: [20457943](https://pubmed.ncbi.nlm.nih.gov/20457943/)
55. Viegas SC, Silva IJ, Saramago M, Domingues S, Arraiano CM (2011) Regulation of the small regulatory RNA MicA by ribonuclease III: a target-dependent pathway. *Nucleic Acids Res* 39: 2918–2930. doi: [10.1093/nar/gkq1239](https://doi.org/10.1093/nar/gkq1239) PMID: [21138960](https://pubmed.ncbi.nlm.nih.gov/21138960/)
56. Afonyushkin T, Vecerek B, Moll I, Blasi U, Kaberdin VR (2005) Both RNase E and RNase III control the stability of *sodB* mRNA upon translational inhibition by the small regulatory RNA RyhB. *Nucleic Acids Res* 33: 1678–1689. doi: [10.1093/nar/gki313](https://doi.org/10.1093/nar/gki313) PMID: [15781494](https://pubmed.ncbi.nlm.nih.gov/15781494/)
57. Marchais A, Duperrier S, Durand S, Gautheret D, Stragier P (2011) CsfG, a sporulation-specific, small non-coding RNA highly conserved in endospore formers. *RNA Biol* 8: 358–364. doi: [10.4161/ma.8.3.14998](https://doi.org/10.4161/ma.8.3.14998) PMID: [21532344](https://pubmed.ncbi.nlm.nih.gov/21532344/)
58. Guerout-Fleury AM, Shazand K, Frandsen N, Stragier P (1995) Antibiotic-resistance cassettes for *Bacillus subtilis*. *Gene* 167: 335–336. PMID: [8566804](https://pubmed.ncbi.nlm.nih.gov/8566804/)
59. Britton RA, Wen T, Schaefer L, Pellegrini O, Uicker WC, et al. (2007) Maturation of the 5' end of *Bacillus subtilis* 16S rRNA by the essential ribonuclease YkqC/RNase J1. *Mol Microbiol* 63: 127–138. PMID: [17229210](https://pubmed.ncbi.nlm.nih.gov/17229210/)
60. Bechhofer DH, Oussenko IA, Deikus G, Yao S, Mathy N, et al. (2008) Analysis of mRNA decay in *Bacillus subtilis*. *Methods Enzymol* 447: 259–276. doi: [10.1016/S0076-6879\(08\)02214-3](https://doi.org/10.1016/S0076-6879(08)02214-3) PMID: [19161848](https://pubmed.ncbi.nlm.nih.gov/19161848/)
61. Stead MB, Agrawal A, Bowden KE, Nasir R, Mohanty BK, et al. (2012) RNAsnap: a rapid, quantitative and inexpensive, method for isolating total RNA from bacteria. *Nucleic Acids Res* 40: e156. doi: [10.1093/nar/gks680](https://doi.org/10.1093/nar/gks680) PMID: [22821568](https://pubmed.ncbi.nlm.nih.gov/22821568/)

62. Smyth GK (2004) Linear models and empirical bayes methods for assessing differential expression in microarray experiments. *Stat Appl Genet Mol Biol* 3: Article3. PMID: [16646809](#)
63. Strimmer K (2008) A unified approach to false discovery rate estimation. *BMC Bioinformatics* 9: 303. doi: [10.1186/1471-2105-9-303](#) PMID: [18613966](#)
64. Zybaylov B, Coleman MK, Florens L, Washburn MP (2005) Correlation of relative abundance ratios derived from peptide ion chromatograms and spectrum counting for quantitative proteomic analysis using stable isotope labeling. *Anal Chem* 77: 6218–6224. PMID: [16194081](#)
65. Bauer KM, Lambert PA, Hummon AB (2012) Comparative label-free LC-MS/MS analysis of colorectal adenocarcinoma and metastatic cells treated with 5-fluorouracil. *Proteomics* 12: 1928–1937. doi: [10.1002/pmic.201200041](#) PMID: [22623418](#)
66. Fechter P, Chevalier C, Yusupova G, Yusupov M, Romby P, et al. (2009) Ribosomal initiation complexes probed by toeprinting and effect of trans-acting translational regulators in bacteria. *Methods Mol Biol* 540: 247–263. doi: [10.1007/978-1-59745-558-9_18](#) PMID: [19381565](#)
67. Chevalier C, Geissmann T, Helfer AC, Romby P (2009) Probing mRNA structure and sRNA-mRNA interactions in bacteria using enzymes and lead(II). *Methods Mol Biol* 540: 215–232. doi: [10.1007/978-1-59745-558-9_16](#) PMID: [19381563](#)